

Hamilton Dynamics in Chemical Reactions: the Maupertuis Principle, Transition Paths and Energy Landscape

Yuan Gao* and Yufan Zhou

*Department of Mathematics, Purdue University, West Lafayette,
Indiana, USA.*

Received 22 April 2023; Accepted 3 May 2023

Abstract. In this paper, we explore the Hamilton structures in non-equilibrium chemical reactions, which is modeled as a random time-changed Poisson process on countable states. Transition paths between multiple steady states in a chemical reaction is a rare event that can be characterized via the large deviation principle. Compared with the Hamilton principle, we use the Maupertuis principle to compute the transition paths and the associated energy barriers, i.e., the rate function in the large deviation principle. Based on the corresponding stationary Hamilton-Jacobi equation, we select a proper stationary viscosity solution, which in general is not unique, to explicitly compute the energy barriers and the associated optimal control that realizes a transition path. Using one-dimensional example, we characterize the energy barriers for chemical reactions using a geometric quantity in the phase plane. We also compare the reaction barriers with the one in the diffusion approximation and show that the global energy landscape and energy barriers for non-equilibrium chemical reactions are quite different with its diffusion approximation.

AMS subject classifications: 49L99, 80A30, 49N99

Key words: Large deviation principle, thermodynamic limit, transition time, energy barriers, infinite time horizon.

*Corresponding author. *Email addresses:* gao662@purdue.edu (Y. Gao), zhou1187@purdue.edu (Y. Zhou)

1 Introduction

Chemical reactions are very important for living matters and also have many industry applications [1, 20, 31, 35, 36]. For various chemical reactions, the most important questions are how the reactions happen along a transition path and how fast they happen. Particularly, non-equilibrium chemical reactions have multiple steady chemical states and the global energy landscape is non-convex and unknown. Compared with equilibrium reactions, the most distinguished feature of non-equilibrium chemical reactions is the positive entropy production rate [30, 32], which can be used as the characterization of living cells. For those non-equilibrium chemical reactions, the above two questions are not only fundamental in the study of non-equilibrium physical processes [10, 30], but also mathematically challenging [2, 11].

A convenient stochastic model to describe a chemical reaction is a random time-changed Poisson process on countable states (see (2.3)) [1, 17, 25]. From this continuous time discrete state Markov process, there are many quantitative properties that can be characterized via the probability limiting theorems for the chemical reaction. For instance, the reaction rate equation, which was proposed in 1864 by Guldberg and Waage, can be viewed as an ensemble path following the law of large numbers. More importantly, the transitions from one stable chemical state to another stable chemical state can be viewed as rare events in the large deviation regime. Rare events happen with very small probability, but they are usually the most important events, for instance the transitions described above.

Based on the stochastic model for chemical reactions, one can further assume the container where chemical reaction happens is very large $V = 1/h \gg 1$. Thus in a macroscopic scale, we will give answers for how to find transition paths, how to compute the energy barrier for a transition path to happen, and what is the transition rate. First, to estimate the very small probability for transitions to happen, we explore the Hamiltonian structures in chemical reactions. Via WKB reformulations [12, 24], the Kolmogorov forward equation becomes a discrete Hamilton-Jacobi equation (HJE). If taking $V \rightarrow +\infty$, then the limiting HJE has an associated Hamiltonian $H(p, x)$ (see (2.8)). The Hamilton dynamics in terms of this Hamiltonian can be used to describe some least action trajectories in the state space [6]. Moreover, the reaction rate Eq. (2.2) can be viewed as a special trajectory for this Hamilton dynamics $p \equiv 0$. It has been proved that the rate function for the large deviation principle at fixed time of the chemical reactions can be computed via the dynamics solution to the corresponding HJE [16].

However, whether one should use the least action principle with a fixed terminal time (the Hamilton principle) or the least action principle with an undefined

terminal time (the Maupertuis principle) is an arguable question. In Section 3, we review and compare the Hamilton principle and the Maupertuis principle using one-dimensional examples. We numerically show the monotonicity for action cost against terminal time and action cost against initial momentum. The least action cost with undefined terminal time is indeed smaller than the one with fixed terminal time. Thus we conclude that computing the transition path in chemical reactions associated with the minimum energy cost should use the Maupertuis principle with the critical energy level zero. The critical energy level is zero because of the special properties of the Hamiltonians for drift-diffusion processes and chemical reaction processes (see Section 3.1). Furthermore, numerical simulations in Section 3.2 show a downhill process in a drift-diffusion process with no control admits zero cost; however, one in classical mechanics dynamics always requires an action cost strictly larger than zero.

As we have seen, the least action cost function in the infinite time horizon can be used to compute the energy barrier in chemical reactions. It is well known that this cost function solves a stationary HJE. However, it is challenging to select a meaningful stationary solution to the corresponding HJE, because the solutions are not unique [4, 15, 18]. In Section 4, we observe that a good candidate as a selected stationary solution shall also serve as a global energy landscape of the Hamilton dynamics of the chemical reactions. This energy landscape is extremely important, particularly for non-equilibrium chemical reactions. One reason is that it can be used to compute the energy barrier of a chemical reaction, and the other reason is that we expect this energy landscape to be also the rate function for the large deviation principle of invariant measures for chemical reactions, which captures all the asymptotic behaviors nearby steady states in a chemical reaction. However, the later observation is only done via numerical experiments, since the invariant measures for non-equilibrium reaction is unknown, and the large deviation principle is still an open question. In Theorem 4.1, we use the maximal Lipschitz viscosity solution starting from a stable steady solution to compute the uphill transition path and the associated the least action cost from that stable states to any other points. Meanwhile, the explicit global energy landscape is found for the Schlögl catalysis model [34], which gives a gradient flow structure with respect to a double well potential. Moreover, numerical simulations show that in Schlögl catalysis model the least action cost along a downhill path admits zero action cost; however, the least action cost along an uphill path always admits an action cost strictly larger than zero.

Diffusion approximation for chemical reactions was originally studied by the celebrated work of Kramer [23], in which the transition rate was computed via the large deviation principle for a drift-diffusion approximation (see also [5]). We

also compare the chemical reactions with its diffusion approximation that shares the same reaction rate equation. However, both the explicit formulas and the geometric interpretations for the energy barrier of the transition paths connecting two states are different: Fig. 16 plot (c) shows the transition rates are not consistent, and Fig. 16 plot (d) shows the least action costs differ by more than ten times. This shows that the diffusion approximation is not an accurate model when computing the energy barrier for chemical reactions, particularly for events in the large deviation regime.

Although numerical methods for simulating transition paths and approximating the associated minimum energy barrier are not our focuses, we refer to [9,28] for the abstract transition path theory and to [7,8,13,19,27,33] for numerical methods for constructing a global energy landscape and the transition paths. Instead of constructing a diffusion approximation or finding an optimal control directly for the jump processes, our method is to first find the selected stationary solution $\psi(x)$ to the limiting HJE, then we use it to construct an exact optimal control $p^*(x) = \nabla\psi(x^*)$ in computing a transition path and an energy barrier.

The remaining contents of this paper are organized as follows. In Section 2, we will describe some preliminary results including the stochastic model and its Hamilton structure induced by WKB expansion. In Section 3, we compare the Hamilton principle and the Maupertuis principle for classical mechanics and the Hamilton dynamics for the diffusion process. In Section 4, we compute the transition path, the energy barrier, and the transition time for chemical reactions. We also compute these for the diffusion approximation of the chemical reactions. At last we give conclusions in Section 5, followed by an Appendix A for elementary proofs of lemmas.

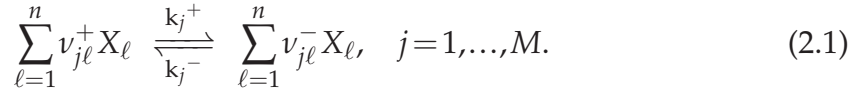
2 The Hamilton structure in chemical reactions

In this section, we first review the stochastic model for chemical reactions and derive the associated HJE via the WKB expansion. The dynamics solution to the dynamics HJE is the rate function in the large deviation principle for fixed time while the large deviation principle for the invariant measure of the chemical reaction is formally related to one stationary solution to HJE, in which the rigorous proof is still open.

2.1 Review of reaction rate equation and the stochastic modeling

We first review the chemical reactions for n species $X_i(t), i = 1, \dots, n$, happening

in a large container characterized by a size $1/h \gg 1$. Assume there are totally M reactions described by the chemical reaction equation



Here $k_j^\pm \geq 0$ is the reaction rate for the forward and backward j -th reaction. From now on, the net changes for the molecular numbers of species for the j -th reaction is denoted as $\vec{v}_j = \vec{v}_j^- - \vec{v}_j^+$.

It is well known that the reaction rate equation for the rate of change of the concentration $\vec{x} = (x_\ell)_{\ell=1:n}$ of each species X_ℓ is proposed by Guldberg and Waage in 1864

$$\frac{d}{dt} \vec{x} = \sum_{j=1}^M \vec{v}_j (\Phi_j^+(\vec{x}) - \Phi_j^-(\vec{x})). \tag{2.2}$$

Here the reaction rate satisfies the law of mass action (LMA)

$$\Phi_j^\pm(\vec{x}) = k_j^\pm \prod_{\ell=1}^n x_\ell^{\nu_{j\ell}^\pm}.$$

However, for a general reaction rate equation, without any gradient flow structure, it is hard to predict the dynamics, the non-equilibrium steady states, the stability and so on. While the more realistic and difficult goals are to find the reaction rates, the transition path and the energy barriers needed for a chemical reaction system. All these questions require the discovery of more mathematical structures from the chemical reactions.

One convenient way to model chemical reactions is using a stochastic counting process. Consider a continuous time Markov process on countable states that counts the number of molecular species $X_i(t), i=1, \dots, n$ for chemical reactions in a container with typical size $1/h$. The rescaled process $X^h(t) = hX(t)$ satisfies

$$X^h(t) = X^h(0) + \sum_{j=1}^M \vec{v}_j h \left(Y_j^+ \left(\frac{1}{h} \int_0^t \Phi_j^+(X^h(s)) ds \right) - Y_j^- \left(\frac{1}{h} \int_0^t \Phi_j^-(X^h(s)) ds \right) \right), \tag{2.3}$$

where $Y_j^\pm(t)$ are i.i.d. unit rate Poisson processes.

By the martingale property of Poisson process, one can derive the chemical master equation, c.f. [14]. For $\vec{x}_i \in \Omega_h := \{\vec{x}_i = i\vec{h}, i \in \mathbb{Z}^n\}$

$$\begin{aligned} \frac{d}{dt} p_h(\vec{x}_i, t) &= \frac{1}{h} \sum_{\substack{j=1, \\ \vec{x}_i - \vec{v}_j h \geq 0}}^M (\Phi_j^+(\vec{x}_i - \vec{v}_j h) p_h(\vec{x}_i - \vec{v}_j h, t) - \Phi_j^-(\vec{x}_i) p_h(\vec{x}_i, t)) \\ &\quad + \frac{1}{h} \sum_{\substack{j=1, \\ \vec{x}_i + \vec{v}_j h \geq 0}}^M (\Phi_j^-(\vec{x}_i + \vec{v}_j h) p_h(\vec{x}_i + \vec{v}_j h, t) - \Phi_j^+(\vec{x}_i) p_h(\vec{x}_i, t)) \end{aligned}$$

for $\vec{x}_i \in \Omega_h^+$.

Without loss of generality, one can identify the backward reaction as a new reaction with a new index and a new reaction vector. Denote

$$\rho_k^h = \rho_h(\vec{x}_k, t), \quad f_k^h = f^h(\vec{x}_k),$$

where $\vec{x}_k = \vec{x}_i + \vec{v}_j h$,

$$Q_{ki}^h := \sum_{j: \vec{x}_k = \vec{x}_i + \vec{v}_j h} \frac{1}{h} \Phi_j(\vec{x}_i + \vec{v}_j h), \quad Q_{ii}^h := -\sum_k Q_{ik}^h$$

for $i = 1, \dots, n, k = 1, \dots, n$. Then the master equation can be rewritten symbolically using the Q -matrix

$$\frac{d}{dt} p_i^h = \sum_{k=1}^n Q_{ki}^h p_k^h = \sum_{k=1}^n (Q_{ki}^h p_k^h - Q_{ik}^h p_i^h), \quad (2.4)$$

where one can redefine $Q_{ii}^h = -\sum_{k=1}^n Q_{ik}^h$ to ensure the row sum zero condition.

On the other hand, let $f^h \in C_b(\Omega_h)$, one can also derive the backward equation for f_i^h

$$\frac{d}{dt} f_i^h = \sum_{k=1}^n Q_{ik}^h (f_k^h - f_i^h) = \sum_{k=1, k \neq i}^n Q_{ik}^h (f_k^h - f_i^h). \quad (2.5)$$

2.2 WKB expansion and the limiting HJE for the chemical reaction compared with diffusion process

To study the quantitative properties, particularly the reaction rates, the transition path, and the energy barriers needed for a chemical reaction system, one need to estimate the small probability $p_h(\vec{x}_i)$ at an unlikely state \vec{x}_i . This unlikely state can be a saddle point or a transition state in the chemical reaction.

Thus we use a WKB reformulation (a change of variable)

$$p^h(\vec{x}_i) = e^{-\frac{\psi_i^h}{h}} \quad (2.6)$$

to derive the dynamics for $\psi_i^h = \psi^h(\vec{x}_i)$. Plugging this into the forward Eq. (2.4), we obtain

$$\partial_t \psi^h(\vec{x}_i) = -h e^{\frac{\psi^h(\vec{x}_i, t)}{h}} Q_h^* e^{-\frac{\psi^h(\vec{x}_i, t)}{h}} =: -H_h^*(\psi^h),$$

where

$$H_h^*(\psi^h) := \sum_j \Phi_j(\vec{x}_i - \vec{v}_j h) e^{\frac{\psi^h(\vec{x}_i) - \psi^h(\vec{x}_i - \vec{v}_j h)}{h}} - \Phi_j(\vec{x}_i).$$

One can do exactly the same WKB reformulation

$$f^h(\vec{x}_i) = e^{\frac{u_i^h}{h}} \quad (2.7)$$

with $u_i^h = u^h(\vec{x}_i)$ for the backward Eq. (2.5). We obtain

$$\partial_t u_h(\vec{x}_i, t) = h e^{-\frac{u_h(\vec{x}_i, t)}{h}} Q_h e^{\frac{u_h(\vec{x}_i, t)}{h}} =: H_h(u_h),$$

where the discrete Hamiltonian is

$$H_h(\vec{x}_i, u_h(\vec{x}_i), u_h) := \sum_{j=1}^M \Phi_j(\vec{x}_i) \left(e^{\frac{u_h(\vec{x}_i + \vec{v}_j h) - u_h(\vec{x}_i)}{h}} - 1 \right).$$

2.2.1 Limiting Hamiltonian and HJE

When one takes the noise level $h \rightarrow 0$, then one can formally obtain a macroscopic HJE in the continuum state space. The rigorous limit from the solution to the discrete HJE to the limiting HJE implies the large deviation principle at various levels, which will be explained in the next section.

First, as $h \rightarrow 0$, we assume $\vec{x}_i \rightarrow \vec{x}$. Then formally taking limit in the discrete Hamiltonian H_h^* implies the macroscopic Hamiltonian for chemical reactions

$$H(\vec{p}, \vec{x}) := \sum_{j=1}^M \Phi_j(\vec{x}) (e^{\vec{v}_j \cdot \vec{p}} - 1) \quad (2.8)$$

and the corresponding HJE on continuous state space

$$\partial_t \psi(\vec{x}, t) = -H(\nabla \psi(\vec{x}), \vec{x}). \quad (2.9)$$

Second, with exactly the same procedure and the same Hamiltonian, as $h \rightarrow 0$, the discrete HJE for the backward equation becomes

$$\partial_t u(\vec{x}, t) = H(\nabla u(\vec{x}), \vec{x}). \quad (2.10)$$

From now on, we drop the vector notation and replace \vec{x}, \vec{p} by x, p if there is no confusion.

2.2.2 Compared with the HJE for drift-diffusion process

As a comparison, consider the Langevin dynamics

$$dX_t = b(X_t)dt + \sqrt{2\varepsilon}dB_t, \quad (2.11)$$

where B_t is n -dimensional Brownian motion. We do the same WKB reformulation $\rho(x,t) = e^{-\psi(x,t)/\varepsilon}$ in the forward equation for the Langevin dynamics (also known as the drift-diffusion process)

$$\partial_t \rho + \nabla \cdot (\rho b) = \varepsilon \Delta \rho. \quad (2.12)$$

The resulting ε -HJE is given by

$$\partial_t \psi = \varepsilon(\nabla \cdot b + \Delta \psi) - \nabla \psi \cdot (b + \nabla \psi). \quad (2.13)$$

Denote the Hamiltonian for drift-diffusion process as

$$H(p, x) := p \cdot (p + b). \quad (2.14)$$

Then we have formally a limiting HJE as $\varepsilon \rightarrow 0$

$$\partial_t \psi(x, t) + H(\nabla \psi(x, t), x) = 0. \quad (2.15)$$

Similarly, in the forward equation for a drift-diffusion process

$$\partial_t f - b \cdot \nabla f = \varepsilon \Delta f, \quad (2.16)$$

the WKB reformulation is $u = e^{f/\varepsilon}$. The resulting ε -HJE is given by

$$\partial_t u(x, t) = H(\nabla u(x, t), x) + \varepsilon \Delta u(x, t). \quad (2.17)$$

Taking $\varepsilon \rightarrow 0$, we formally obtain the same HJE with only a sign difference

$$\partial_t u(x, t) - H(\nabla u(x, t), x) = 0. \quad (2.18)$$

2.3 The large deviation rate function derived from dynamic/stationary HJE

The above WKB expansion for the time marginal probability density function $\rho(x, t)$ gives a formal estimate on the smallness of the time marginal probability density. More explicitly, the dynamic solution $\psi(x, t)$ to the HJE (2.9) gives the exponential rate estimate for the time marginal probability density $\rho(x, t)$.

However, the rigorous justification for the large deviation rate function for process X^h at fixed time t needs to be proved by the inverse Varadhan's lemma [3]. In detail,

(i) one needs to prove the Varadhan’s nonlinear semigroup

$$\begin{aligned} u_h(x_i, t) &= h \log f^h(x_i, t) = h \log \mathbb{E}^{x_i}(f_0(X_t^h)) \\ &= h \log \mathbb{E}^{x_i}\left(e^{\frac{u_0(X_t^h)}{h}}\right) =: (S_t u_0)(x_i) \end{aligned} \tag{2.19}$$

converges to the viscosity solution of the dynamic HJE (2.10). Here f_0 is the initial condition for the backward Eq. (2.5) and u_0 is the initial condition for the HJE (2.10).

(ii) One needs to prove the tightness of X^h at fixed time t .

In (i), notice the Lax-Oleinik semigroup representation for the viscosity solution to (2.10) is

$$\begin{aligned} u(x, t) &= \sup_y (u_0(y) - J(y; x, t)), \\ J(y; x, t) &:= \inf_{\substack{\gamma(0)=x, \\ \gamma(t)=y}} \int_0^t L(\dot{\gamma}(s), \gamma(s)) \, ds, \end{aligned} \tag{2.20}$$

where $L(s, x)$ is the convex conjugate of $H(p, x)$ in terms of p . Then the convergence of $\lim_{h \rightarrow 0} u_h = u$ gives the variational characterization for the rate function $J(y; x, t)$, i.e., Varadhan’s lemma

$$\lim_{h \rightarrow 0} h \log \mathbb{E}^{x_i}\left(e^{\frac{u_0(X_t^h)}{h}}\right) = \sup_y (u_0(y) - J(y; x, t)). \tag{2.21}$$

We refer to [16] for the detailed proof of the tightness and the convergence of $\lim_{h \rightarrow 0} u_h = u$ via the method of monotone schemes.

If one considers the long time behavior of HJE (2.10), then the stationary solution $u^*(x)$ as the large time limit of $u(x, t)$ will not be unique because in general, the stationary HJE

$$H(\nabla u(x), x) = 0 \tag{2.22}$$

does not satisfy comparison principle. For instance, the Mane potential defined as

$$J(y; x) := \inf_{t \geq 0} \inf_{\substack{\gamma(0)=x, \\ \gamma(t)=y}} \int_0^t L(\dot{\gamma}(s), \gamma(s)) \, ds \tag{2.23}$$

serves as one viscosity solution to the stationary HJE (2.22). On the other hand, $J(y; x) + C$ for any constant C are also viscosity solutions to (2.22). How to select a meaningful stationary viscosity solution to (2.22) is a long standing open

question. We refer to [4, 18, 21] for the vanishing discount limit method and refer to [15] for the selection principle using the large deviation principle for the invariant measures to the underlying stochastic process, i.e., drift-diffusion process or the chemical reaction processes.

Using the large deviation principle for invariant measures as a selection principle for the stationary HJE has many advantages. First, the corresponding rate function gives a selected meaningful stationary viscosity solution. Second, the rate function in the large deviation principle for invariant measures can capture all the asymptotic behaviors of the original (stochastic) dynamics and thus serve as a global energy landscape of the original dynamics. Third, this energy landscape is extremely important, particularly for non-equilibrium chemical reactions, for the energy barrier and transition rate estimates in the transition path problem. These will be explained in detail with explicit one-dimensional examples.

2.4 The Hamilton structure and the implied RRE for the zero noise limit

With the Hamiltonian for the drift-diffusion process and the chemical reactions, we consider the Hamilton dynamics

$$\dot{x} = \nabla_p H(p, x), \quad \dot{p} = -\nabla_x H(p, x). \quad (2.24)$$

It is well known that for any least action problem for fixed t , the least action curve connecting x^A to y such that

$$J(y; x^A, t) := \inf_{\substack{\gamma(0)=x^A, \\ \gamma(T)=y}} \int_0^T L(\dot{\gamma}(t), \gamma(t)) dt$$

solves the Hamilton dynamics (2.24) with $p = \partial L / \partial s$.

We then observe an important property that $H(0, x) = 0$ for both Hamiltonians (2.14) and (2.8). This property immediately implies that

$$L(s, x) = \sup_p (s \cdot p - H(p, x)) = s \cdot p^* - H(p^*, x) \geq 0 \quad \text{with} \quad s = \partial_p H(p^*, x), \quad (2.25)$$

and the equality holds if and only if $p^* = 0$ because $L(s, x)$ is convex with respect to s .

Therefore, we can conclude that for Hamiltonians (2.14) and (2.8), the zero-cost path is only achieved at

$$\dot{x}(t) = \partial_p H(0, x), \quad p(t) \equiv 0. \quad (2.26)$$

Using this Hamilton structure, the RRE (2.2) can be recast in terms of the Hamiltonian (2.8) for chemical reaction as

$$\dot{x}(t) = \partial_p H(0, x). \quad (2.27)$$

Notice the corresponding Hamiltonian along the zero-cost path is always zero

$$H(p(t), x(t)) \equiv H(0, x(t)) = 0. \quad (2.28)$$

We will refer this path as zero-cost path or downhill path or the RRE path. We also refer to [14] for the statement that this zero-cost path satisfies the law of large numbers for the chemical reaction process X^h .

On the other hand, when $p \neq 0$, there is also a least action path which has a constant zero Hamiltonian but the action cost is larger than zero. We will refer this non-zero cost path as an uphill path or the transition path in the large deviation regime. There are in general two ways to find this path:

- (i) To solve the Hamilton dynamics with specific initial and ending points.
- (ii) To find the PDE solutions to the corresponding dynamic/stationary HJE.

There are some delicate choices on the two methods for different problems. In Section 3, by comparing mechanic Hamiltonian and the Hamiltonian for Langevin dynamics, we study whether one should use the Maupertuis principle or the Hamilton principle when computing the least actions for a transition path in chemical reactions. In Section 4, by comparing details properties for the downhill/uphill transition paths in chemical reactions and its diffusion approximation, we study whether and when one can use the diffusion approximation to compute the transition paths and the transition rate. In this section, we will also demonstrate how the stationary solution to HJE plays the role of the Lyapunov function and the role of the energy landscape in a non-equilibrium chemical reaction. The gradient flow structure and dissipation-conservation decomposition will also be compared for both Langevin dynamics and chemical reactions.

3 Comparisons between the Maupertuis principle and the Hamilton principle

Recall our goal is to study how the Hamilton structure plays a role in finding the reaction rates, the transition paths, and the energy barriers needed for a chemical reaction system.

Given the Hamiltonian and Hamilton dynamics derived in Section 2, we want to find which kind of least action principle we shall use. More specifically, we need first compare the Maupertuis principle and the Hamilton principle for given Hamiltonian and Lagrangian.

3.1 Review of the Hamilton principle and the Maupertuis principle

We first review two different least action principles: the Hamilton principle and the Maupertuis principle.

The Hamilton principle: Given x^A, y and a fixed terminal time T such that $\gamma(0) = x^A, \gamma(T) = y$, then the Hamilton principle reads

$$J(y; x^A, T) := \inf_{\substack{\gamma(0)=x^A, \\ \gamma(T)=y}} \int_0^T L(\dot{\gamma}(t), \gamma(t)) dt. \quad (3.1)$$

This least action principle for fixed time T leads to three consequences:

- (i) The optimal curve $\gamma^*(t), t \in [0, T]$ satisfies Euler-Lagrangian equation

$$\frac{d}{dt} (\partial_s L(\dot{\gamma}(t), \gamma(t))) = \partial_x L(\dot{\gamma}(t), \gamma(t)) \iff \ddot{\gamma} = -\nabla U(\gamma). \quad (3.2)$$

- (ii) The optimal curve satisfies Hamilton dynamics

$$\dot{\gamma} = \partial_p H, \quad \dot{p} = -\partial_x H \quad (3.3)$$

and the dynamics stays within the same energy level $H \equiv c$.

- (iii) The value function $J(y; x^A, T) =: J(y, T)$ satisfies the dynamic HJE

$$\partial_T J + H(\nabla J, y) = 0. \quad (3.4)$$

For the convenience of computations in the later section, we also derive the following equivalent form for the value function $J(y; x^A, T)$. Denote the least action path achieving the minimum value $J(y; x^A, T)$ as $\gamma^*(t)$. Then for the constant $c_H = H(p^*(t), \gamma^*(t)) = H(p^*(0), \gamma^*(0))$, we have

$$\begin{aligned} J(y; x^A, T) + c_H T &= \int_0^T \left(L(\dot{\gamma}^*(t), \gamma^*(t)) + H(p^*(t), \gamma^*(t)) \right) dt \\ &= \int_0^T \partial_p H(p^*(t), \gamma^*(t)) \cdot p^*(t) dt. \end{aligned} \quad (3.5)$$

The Maupertuis principle: Given an energy level c , assume x^A, y belongs to Hill's region $\{x; U(x) \leq c\}$. The Maupertuis principle is to find a least action curve connecting $x(0) = x^A$ to $x(T) = y$ with undefined terminal time T and staying within the same energy level $H(p, x) =: c_H$. Under the assumption of finding curve within the same energy level

$$H(p(t), x(t)) \equiv c_H, \tag{3.6}$$

the Maupertuis principle with an undefined terminal time reads

$$V(y; x^A, c_H) = \inf_{\substack{T>0, \\ \gamma(0)=x^A, \gamma(T)=y}} \int_0^T (L(\dot{\gamma}(t), \gamma(t)) + c_H) dt. \tag{3.7}$$

Then by the Pontryagin maximal principle, one can derive that the least action path solves the Hamilton dynamics up to an optimal terminal time $0 \leq t \leq T^*$, where T^* can be $+\infty$

$$\dot{\gamma} = \partial_p H, \quad \dot{p} = -\partial_x H, \quad H(p(t), x(t)) \equiv c_H. \tag{3.8}$$

Similar to (3.5), along any least action path $\gamma^*(t); 0 \leq t \leq T^*$, the following formula holds, which provides computational convenience:

$$\begin{aligned} V(y; x^A, c_H) &= \int_0^{T^*} (L(\dot{\gamma}^*(t), \gamma^*(t)) + H(p^*(t), \gamma^*(t))) dt \\ &= \int_0^{T^*} \partial_p H(p^*(t), \gamma^*(t)) \cdot p^*(t) dt. \end{aligned} \tag{3.9}$$

Another consequence is that the value function $V(y; x^A, c_H) =: V(y)$ solves the following stationary HJE in the viscosity sense:

$$H(\nabla V(y), y) = c_H. \tag{3.10}$$

Here c_H is the critical energy level such that the least action in (3.7) is well-defined (it is also known as the critical Mañè value). It has been proved that the critical energy level c_H for the Langevin dynamics and the chemical reactions are zero, i.e., $c_H = 0$. Thus for these two Hamiltonians and the least action problems via the Maupertuis principle, we simply take $c_H = 0$ so that the associated stationary HJE becomes

$$H(\nabla V(y), y) = 0. \tag{3.11}$$

3.2 The least action cost under the Maupertuis principle and the Hamilton principle

In this section, we illustrate the least action cost under the Hamilton principle and the Maupertuis principle with examples. We first select an energy landscape for classical mechanics dynamics and Langevin dynamics. Then, with selected energy landscape, numerical simulations will show the symmetry, monotonicity, and downhill/uphill process for two dynamics. Last, in the uphill process, we will find the least action path, under the Hamilton principle and the Maupertuis principle.

3.2.1 The Hamilton dynamics for classical mechanics dynamics and for Langevin dynamics

In this section, we select an energy landscape and then sketch the phase planes for two dynamics. Let $U(x)$ be the energy landscape, then the Hamiltonian for classical mechanics is

$$H(p, x) = \frac{1}{2}|p|^2 + U(x), \quad (3.12)$$

and its convex conjugate, Lagrangian, is

$$L(s, x) = \frac{1}{2}|s|^2 - U(x). \quad (3.13)$$

According to Eq. (3.2), the optimal curve satisfies the system of ordinary differential equations

$$\begin{aligned} \dot{x} &= p, \\ \dot{p} &= -\nabla U(x). \end{aligned} \quad (3.14)$$

According to the Hamilton principle (3.5), the least action connecting x^A and y is expressed with a fixed terminal time

$$J(y; x^A, T) + c_H T = \int_0^T |p^*(t)|^2 dt. \quad (3.15)$$

According to the Maupertuis principle (3.7), the least action connecting x^A and y is expressed with an unfixed terminal time T^*

$$V(y; x^A, c_H) = \int_0^{T^*} |p^*(t)|^2 dt. \quad (3.16)$$

Recall (2.14), we take $b(x) = -\nabla U(x)$. Thus, the Hamiltonian for Langevin dynamics is

$$H(x, p) = p(p - \nabla U(x)), \quad (3.17)$$

and its convex conjugate, Lagrangian, is

$$L(s, x) = \frac{1}{4}|\dot{x} + \nabla U(x)|^2. \quad (3.18)$$

According to the Eq. (3.2), the optimal curve satisfies the system of ordinary differential equations

$$\begin{aligned} \dot{x} &= 2p - \nabla U(x), \\ \dot{p} &= p \Delta U(x). \end{aligned} \quad (3.19)$$

According to the Hamilton principle (3.5), the least action connecting x^A and y is expressed with a fixed terminal time

$$J(y; x^A, T) + c_H T = \int_0^T |p^*(t)|^2 dt. \quad (3.20)$$

Recall that the critical energy level for Langevin dynamics is $c_H=0$. Moreover, according to the Maupertuis principle (3.7), the least action connecting x^A and y is expressed with an unfixed terminal time

$$V(y; x^A, c_H) = \int_0^{T^*} |p^*(t)|^2 dt. \quad (3.21)$$

In order to discuss the energy barrier, we introduce a precise definition of uphill process and downhill process.

Definition 3.1. *Let $(x(t), p(t))$ be a solution of a two-dimensional dynamical system defined in $I \subseteq \mathbb{R}$. If the energy function $U(x)$ monotonically increases in (a, b) , then the solution has an uphill process in (a, b) ; if the energy function $U(x)$ monotonically decreases in (a, b) , then the solution has a downhill process in (a, b) .*

In the following discussion, we will consider a specific energy landscape

$$U(x) = (x^2 - 1)^2. \quad (3.22)$$

The specific Hamiltonian under the energy landscape (3.22) for classical mechanics is

$$H(p, x) = \frac{1}{2}p^2 + (x^2 - 1)^2, \quad (3.23)$$

and the corresponding system of ordinary differential equations is

$$\begin{aligned} \dot{x} &= p, \\ \dot{p} &= 4x - 4x^3. \end{aligned} \quad (3.24)$$

The Hamiltonian under the energy landscape (3.22) for Langevin dynamics is

$$H(p, x) = p(p + 4x - 4x^3), \quad (3.25)$$

and the corresponding system of ordinary differential equations is

$$\begin{aligned} \dot{x} &= 2p + 4x - 4x^3, \\ \dot{p} &= p(12x^2 - 4). \end{aligned} \quad (3.26)$$

Fig. 1 displays two phase plane plots. The left refers to the classical mechanics dynamics (3.24), and the right refers to Langevin dynamics (3.26). The plots depict multiple trajectories represented by different colors. The blue dot represents the starting point of each trajectory, while the red dot represents its end point. Trajectories that are not associated with any point are periodic. These plots reveal important features, including symmetry, periodic orbits, and stability points. Detailed comparisons of these features will be presented in the following section.

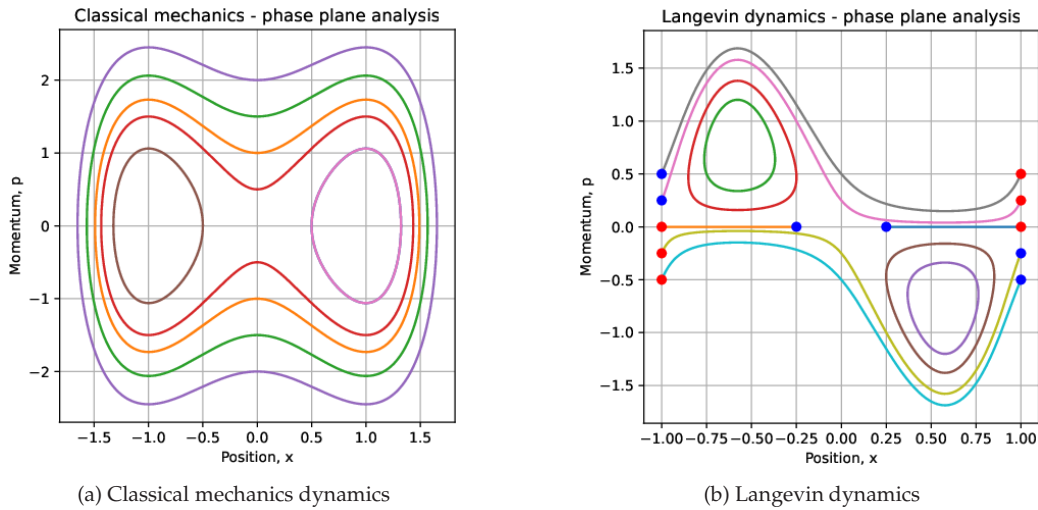


Figure 1: These phase planes are overviews of two systems (3.24) and (3.26). The first graph represents the phase portrait for classical mechanics dynamics, and the second graph displays the Langevin dynamics. To provide a comprehensive view of the directional field, multiple trajectories are included and depicted with varying colors. For a trajectory, the blue dot denotes the starting point, and the red dot denotes the ending point. A trajectory not involved with any point is periodic.

3.2.2 Comparisons for basic properties: Periodicity, symmetry, stability and downhill zero cost path

In this section, we compare basic properties for two dynamics. Then, we will theoretically prove and numerically show the action cost along the downhill path is zero. The basic properties of two dynamics (3.24) and (3.26) are presented as lemmas, and their proofs are provided in the appendix.

Lemma 3.1. *Classical mechanics dynamics (3.24) exhibits symmetry with respect to x -axis and p -axis; it is also symmetric with respect to the origin, i.e.*

$$(i) \quad H(-p, x) = H(p, -x) = H(p, x),$$

$$(ii) \quad H(-p, -x) = H(p, x).$$

Hamilton dynamics (3.26) for Langevin dynamics exhibits symmetry with respect to the origin; moreover, Hamiltonian (3.25) exhibits symmetry with respect to $\nabla U(x)/2$, i.e.,

- (i) $H(-p, -x) = H(p, x)$,
- (ii) $H(\nabla U(x) - p, x) = H(p, x)$.

Lemma 3.2 (Special Property for Classical Mechanics). *Any solution in classical mechanics (3.24) is periodic. Furthermore, the period monotonically decreases with the initial momentum and the initial position.*

Lemma 3.3. *Classical mechanics dynamics (3.24) has 3 steady points: $(1,0)$, $(-1,0)$, and $(0,0)$. Moreover, $(0,0)$ is a saddle point, while $(-1,0)$ and $(1,0)$ are centers.*

The Hamilton dynamics (3.26) for Langevin dynamics has 5 steady points $(0,0)$, $(1,0)$, $(-1,0)$, $(\frac{1}{\sqrt{3}}, -\frac{4}{3\sqrt{3}})$, $(-\frac{1}{\sqrt{3}}, \frac{4}{3\sqrt{3}})$. Moreover, the points $(0,0)$, $(1,0)$, $(-1,0)$ are saddle points, while $(-\frac{1}{\sqrt{3}}, \frac{4}{3\sqrt{3}})$ are centers.

Proposition 3.1 (Special Property for Langevin Dynamics). *Consider the Hamilton dynamics (3.26) for Langevin dynamics. If there exists a downhill path connecting x^A and y such that Hamiltonian $H(p^*(t), x^*(t)) = 0$ for all $t \in (0, T]$, then the action cost along this path is 0.*

Proof. Let $H(p^*(t), x^*(t)) = 0$, then one may obtain two solutions curves: $p^* = 0$ and $p^* = \nabla U(x^*)$.

We show the curve $p^* = \nabla U(x^*)$ is not a downhill path. We plug it into the differential equation $\dot{x} = p$, then we obtain $\dot{x}^* = \nabla U(x^*)$. Multiplying both sides with $\nabla U(x^*)$ and then taking integral with respect to t yield

$$U(x^*(T)) - U(x^*(0)) = \int_0^T (\nabla U(x^*))^2 dt \geq 0.$$

Therefore, $U(x^*(T)) \geq U(x^*(0))$ implies $p^* = \nabla U(x^*)$ is not a downhill path.

Thus the solution that meets the downhill process is $p^*(t) = 0$ for all $t > 0$. Along this curve, the least action connecting x^A and y is

$$J(y; x^A, T) = \int_0^T (p^*(t))^2 dt = 0. \tag{3.27}$$

The proof is complete. □

Fig. 2 displays multiple curves with initial momentum $p_0 = 0$ and varying initial position x_0 in the phase plane. The first plot shows the relation between position x and momentum p , the second plot shows the relation between time t and position x , and the third plot shows the relation between time t and momentum p . The last graph shows the relation between action cost of each curve and the corresponding initial position. From these graphs, one may notice as long as $p_0 = 0$, the momentum always keeps $p = 0$. The action cost is also 0.

Corollary 3.1. *The gradient flow structure of the Hamilton dynamics (3.26) Langevin dynamics is $\dot{x} = -\nabla U(x)$. Thus,*

$$\frac{dU(x)}{dt} = -|\nabla U(x)|^2 \leq 0.$$

In contrast, the dynamics of classical mechanics (3.24) does not have a downhill path along which the action cost is zero. Fig. 3 shows multiple curves with ini-

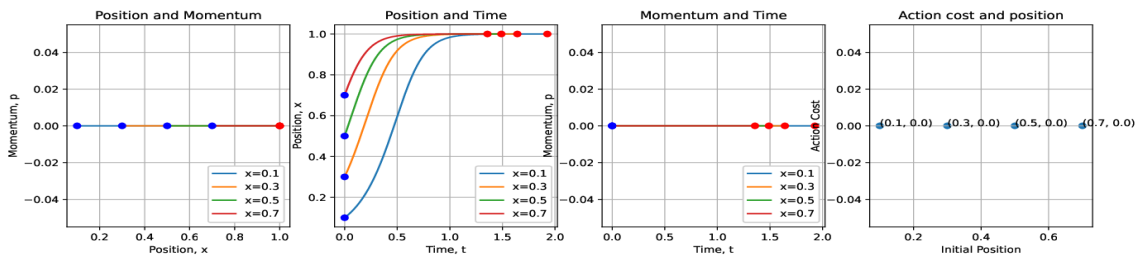


Figure 2: Langevin dynamics: Phase plane for downhill process and action cost. These plots refer to the Hamilton dynamics (3.26) for Langevin dynamics. The first plot shows the relation between position x and momentum p , the second plot shows the relation between time t and position x , and the third plot shows the relation between time t and momentum p . The last graph shows the relation between action cost of each curve and the corresponding initial position. From these graphs, one may notice that the momentum keeps $p = 0$, no matter what the initial position x_0 is. Most importantly, one may notice that the action cost also keeps 0 for different initial position x_0 .

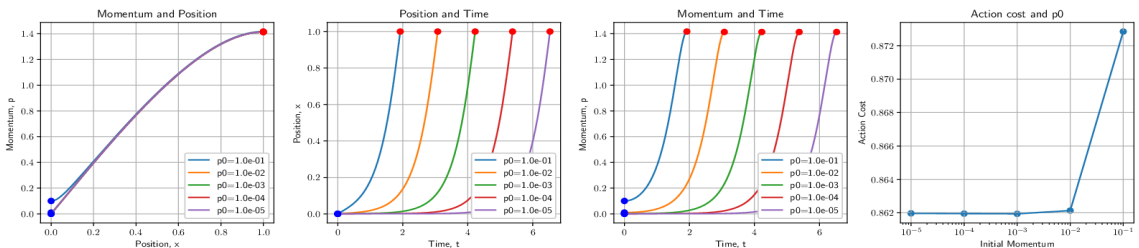


Figure 3: Mechanics dynamics: Phase plane for downhill process and action cost. The plots illustrate the classical mechanics dynamics (3.24). To avoid trivial curves, we consider five different curves with p_0 approaching 0 and varying values of x_0 , as shown in the first three phase plane plots. The last plot displays varying action cost with respect to different initial momenta. From these graphs, we observe that the momentum cannot remain at zero, regardless of how x_0 approaches zero asymptotically. Furthermore, the action cost converges to a positive value of approximately 0.8620.

tial momentum approaching 0 and fixed initial position $x_0=0$ in the phase plane. The first, second, and third plots display the position-momentum, position-time, and momentum-time relationships, respectively. The last graph shows the relationship between the action cost of each curve and its initial momentum p_0 . From these graphs, we observe that the momentum cannot remain at zero, regardless of the initial position x_0 . Additionally, the action cost converges to a positive value of approximately 0.8620.

3.2.3 Comparisons of least action cost: Monotonicity and uphill transition path under the Hamilton principle

As we notice $U(x) = (x^2 - 1)^2$ monotonically increases in $(-1, 1)$, a solution to a dynamical system that meets the boundary condition $x(0) = -1$ and $x(T) = 0$, $T \in (0, +\infty) \cup \{+\infty\}$ corresponds to an uphill process. In this section, we specifically find the least action path and the least action cost connecting $x(0) = -1$ and $x(T) = 0$ under the Hamilton principle and the Maupertuis principle. Proposition 3.2 shows the least action under the Hamilton dynamics. Proposition 3.3 shows the least action under Maupertuis principle. Proposition 3.4 provides the geometric interpretation of the least action cost.

Lemma 3.4. *For classical mechanics dynamics (3.24), if we fix the initial momentum $p_0 > \sqrt{2}$, then the action cost monotonically increases with the k -th arrival time, T_1, T_2, \dots . Furthermore, the action cost monotonically increases with the arrival time.*

Let T_k be the k -th reaching time. We set $p_0 = 1.543024$ such that $T_1 = 1.0$, and proceed to compute T_2 and T_3 . The results are summarized in Fig. 4, which consists of three plots showing the trajectory, arrival time, and the corresponding action cost. The blue dot represents the starting point, and the red dot represents the ending point. Each of the three graphs corresponds to the first three arrivals, respectively. From these graphs, we observe that the action cost monotonically increases with the arrival time.

The following proposition compares the monotonicity of action and momentum under the Hamilton principle.

Proposition 3.2. *For classical mechanics dynamics (3.24) and the Hamilton dynamics (3.26) for Langevin dynamics, if we fix terminal time as $T = 1$, then the terminal position and the action cost monotonically increase with the initial momentum p_0 .*

Fig. 5 shows the uphill path of classical mechanics dynamics (3.24) under the Hamilton principle. The first three plots show relations for position/momentum, time/position, and time/momentum, respectively. The last plot shows the relation for action cost and the initial momentum. With fixed motion of time $T=1$

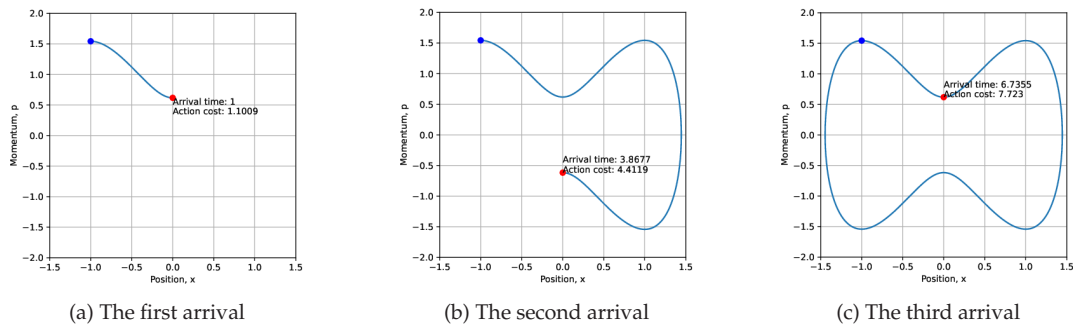


Figure 4: Mechanics dynamics: Three arrivals and corresponding action cost. Three graphs refer to classical mechanics (3.24). Given fixed initial momentum $p_0 = 1.5430$, they show phase portraits for different arrival time and the corresponding action costs. From three graphs, one may observe the action cost monotonically increases with the arrival time.

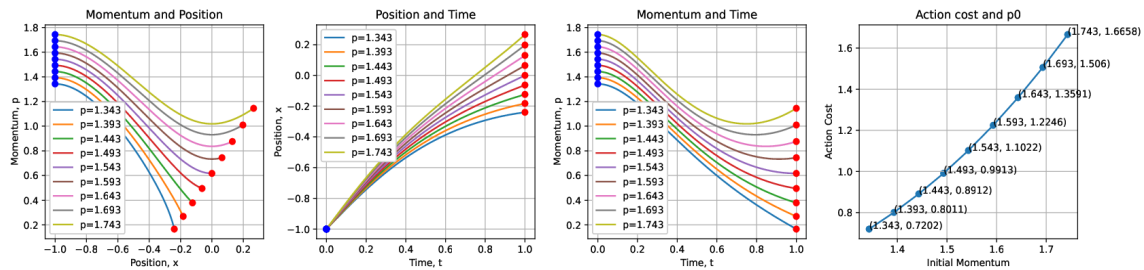


Figure 5: Mechanics dynamics under the Hamilton principle: Phase plane for uphill process and corresponding action cost. In terms of classical mechanics dynamics (3.24), these plots depict the relationships between the position/momentum, position/time, and momentum/time, as well as the correlation between the action cost and the initial momentum. The plots display nine curves with varying initial momenta, showing that the final position, momentum, and action cost consistently increase with the initial momentum.

and initial position $x_0 = -1$, nine curves with different initial momentum p_0 are included. From these graphs, one may observe that the terminal position, terminal momentum, and action cost monotonically increase with initial momentum p_0 .

Fig. 6 illustrates the path followed by the Hamilton dynamics (3.26) for Langevin dynamics, adhering to the Hamilton principle. The first three plots depict the relationships between the position/momentum, position/time, and momentum/time, respectively. The last plot shows the correlation between the action cost and the initial momentum. The plots display nine curves with varying initial momenta p_0 , keeping the fixed terminal time as $T = 1$ and the initial position at $x_0 = -1$. These curves demonstrate that the final position, final momentum, and action cost consistently increase as the initial momentum p_0 increases. Therefore, these results provide evidence of a monotonically increasing relationship between the initial momentum and the terminal position, momentum, and action cost.

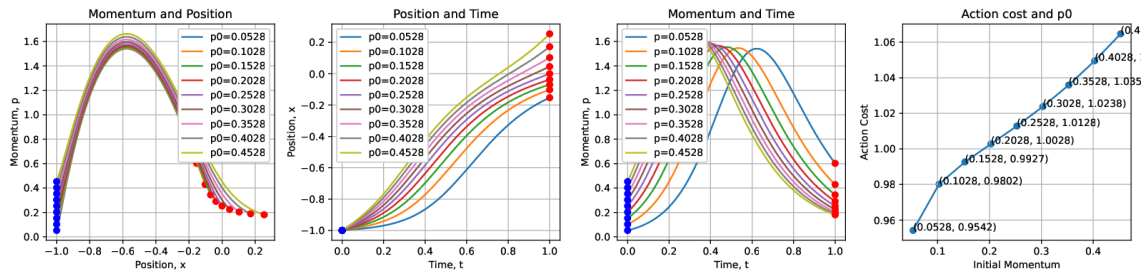


Figure 6: Langevin dynamics under the Hamilton principle: Phase plane for uphill process with fixed terminal time and corresponding action cost. Four plots are for the Hamilton dynamics (3.26) for Langevin dynamics. Nine curves with initial momentum interval $\Delta p = 0.05$ are included with different colors. The last plot depicts the relation between action cost and initial momentum p_0 . From these graphs, one may observe that the terminal position, terminal momentum, and action cost monotonically increase with initial momentum p_0 .

Proposition 3.3. For classical mechanics dynamics (3.24) and the Hamilton dynamics (3.26) for Langevin dynamics, if we fix terminal position as $x = 0$, then the terminal time monotonically decreases with initial momentum p_0 , and the action cost monotonically increases with the initial momentum p_0 .

Fig. 7 illustrates the uphill path of classical mechanics dynamics (3.24) under fixed terminal position and unfixed terminal time. The first three plots depict the relationships between the position/momentum, position/time, and momentum/time, while the last plot shows the correlation between the action cost and the initial momentum. These plots include nine curves with varying initial momenta p_0 , keeping the initial position fixed at $x_0 = -1$ and the terminal position at $x = 0$. The curves demonstrate that the terminal momentum and action cost consistently increase as the initial momentum p_0 increases. Therefore, the results provide evidence of a monotonically increasing relationship between the initial

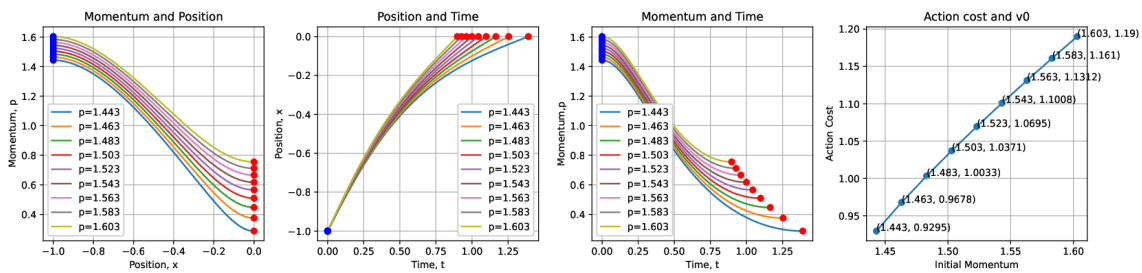


Figure 7: Mechanics dynamics under fixed terminal position and unfixed terminal time: Phase plane for uphill process and corresponding action cost. The plots depict the relationships between position/momentum, position/time, momentum/time, and the action cost/initial momentum. Results show a consistent increase in the terminal momentum and action cost with an increase in initial momentum, while the arrival time decreases with initial momentum.

momentum, the terminal momentum, and the action cost.

Fig. 8 illustrates the uphill path of the Hamilton dynamics (3.26) for the Langevin dynamics under fixed terminal position and unfixed terminal time. Four plots represent the relationships between position/momentum, position/time, momentum/time, and action cost/initial momentum. The plots include nine curves with varying initial momenta, maintaining a fixed initial position and terminal position. The findings indicate a consistent increase in the terminal momentum and action cost with an increase in initial momentum. Thus, the initial momentum has a monotonically increasing relationship with the terminal momentum and action cost.

It motivates the Maupertuis principle for two dynamics.

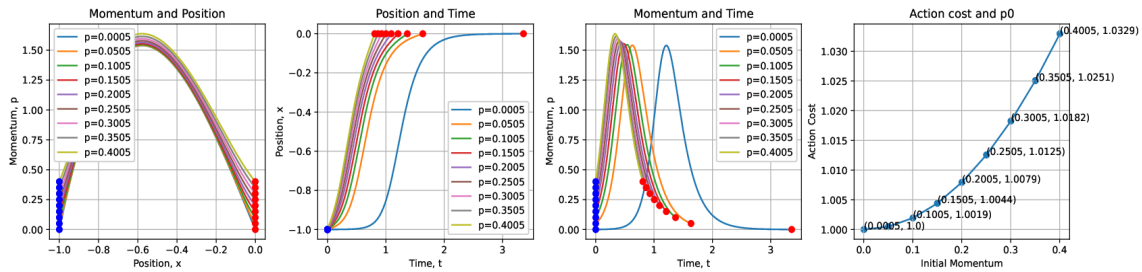


Figure 8: Langevin dynamics under fixed terminal position and unfixed terminal time: Phase plane for uphill process and corresponding action cost. The four plots depict the Hamilton dynamics (3.26) for the Langevin dynamics with nine curves representing different initial momenta p_0 , each denoted by a different color and with an initial momentum interval of $\Delta p = 0.05$. The results show that the terminal momentum and action cost increase monotonically with the initial momentum p_0 , while the arrival time decreases monotonically with the initial momentum p_0 .

3.2.4 Comparisons of least action cost: Uphill transition path and transition rate under the Maupertuis principle

In the following proposition, we give the explicit formula for the least action cost for Langevin dynamics (3.26). Compared with it, the mechanics dynamics do not have an explicit formula.

Proposition 3.4 (Mechanics v.s. Langevin). *For Langevin dynamics (3.26), if $U'(x^A) = 0$ and there is no other critical points between x^A and y , we have an explicit uphill action cost formula for least action curve starting from x^A to y*

$$V(y; x^A, 0) = U(y) - U(x^A). \tag{3.28}$$

However, for mechanics dynamics (3.24), we do not have explicit formula for the uphill action cost.

Fig. 9 illustrates the uphill process of classical mechanics dynamics (3.24) with fixed terminal position and unfixed terminal time. The four plots show the relationships between position/momentum, position/time, momentum/time, and action cost/initial momentum. The plots include five curves with varying initial momenta, while the initial and terminal positions remain fixed. The results reveal that as the initial momentum p_0 approaches $\sqrt{2}$, the required terminal time approaches infinity. Under the Maupertuis principle, the initial momentum approaches $\sqrt{2}$, and the least action connecting $x = -1$ and $x = 0$ converges to a positive value of approximately 0.8619.

Fig. 10 illustrates the uphill process of the Hamilton dynamics (3.26) for the Langevin dynamics with fixed terminal position and unfixed terminal time. The four plots show the relationships between position/momentum, position/time, momentum/time, and action cost/initial momentum. The plots include five curves with varying initial momenta, while the initial and terminal positions remain re-

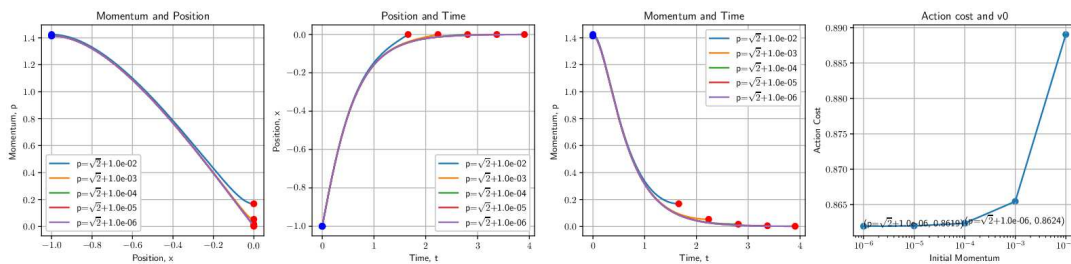


Figure 9: Mechanics dynamics under the Maupertuis principle: Phase plane for uphill process and the least action cost. Four plots are for classical Mechanics dynamics (3.24). The four plots show the relationships between position/momentum, position/time, momentum/time, and action cost/initial momentum. The plots include five curves with varying initial momenta, while the initial and terminal positions remain fixed. From these graphs, one may observe the action cost converges to approximately 0.8619, as the initial momentum approaches to $\sqrt{2}$.

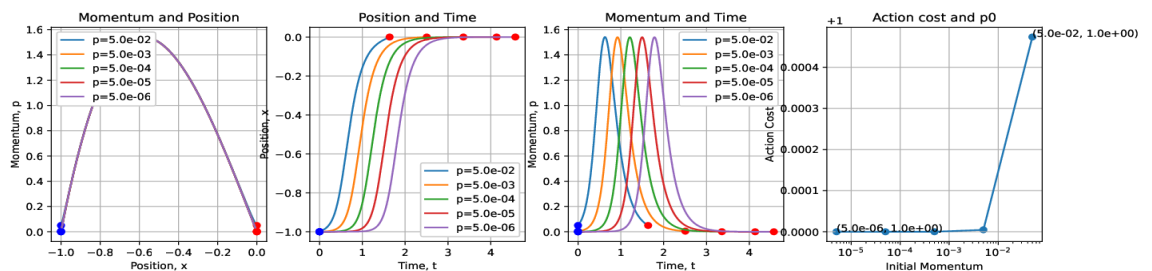
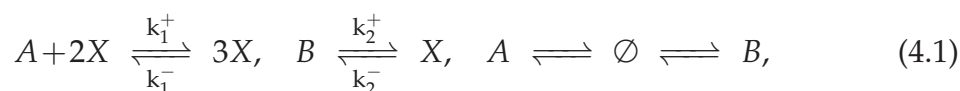


Figure 10: Langevin dynamics under the Maupertuis principle: Phase plane for uphill process and the least action cost. Four plots are for the Hamilton dynamics (3.26) for the Langevin dynamics. Fives curves with different initial momentum are included with different colors. Under the Maupertuis principle, the initial momentum asymptotically approaches to 0, and the action cost approximately converges to the least action cost. Moreover, the least action connecting -1 and 0 cost is 1.

main fixed. The results reveal that as the initial momentum p_0 approaches 0, the required terminal time approaches infinity. Under the Maupertuis principle, the initial momentum approaches 0, and the least action connecting $x = -1$ and $x = 0$ converges to a positive value of approximately 1.00.

4 Comparisons between chemical reaction with its diffusion approximation

In this section, we consider Schlögl catalysis model [34] with environment \emptyset , chemostats A, B and internal specie X



where $k_1^+, k_1^-, k_2^+, k_2^- > 0$ are reaction rates. Based on the Maupertuis principle, we will find out the transition paths, the transition rate and the least action cost for the chemical reactions, with particular focus on the Schlögl catalysis model. We also prove an abstract theorem on the implications of the stationary solution to the stationary HJE. Theorem 4.1 can be used to compute the explicit transition path and transition cost, which is also related to the area enclosed by least action curves in the phase plane, see Proposition 4.3. Moreover, with both explicit formulas and detailed numerical simulations, we compare those quantitative properties for the chemical reactions with its diffusion approximation and conclude that diffusion approximation is not accurate for computing the energy barrier associated with the transition paths.

4.1 The Hamilton dynamics for chemical reaction Hamiltonian and for Langenvin Hamiltonian

In this section, we focus on the Hamilton dynamics for Schlögl catalysis model and the Hamilton dynamics for its diffusion approximation. Based on this example, we revisit the Maupertuis principle for chemical reactions and show a phase plane plots for both two Hamilton dynamics.

4.1.1 Hamilton dynamics and basic properties

From the derivation of (2.8) in Section 2, the Hamiltonian for Schlögl catalysis model is

$$H(p, x) = (k_1^+ ax^2 + k_2^+ b)(e^p - 1) + (k_1^- x^3 + k_2^- x)(e^{-p} - 1). \quad (4.2)$$

With parameters $k_1^+ a = 6, k_2^+ b = 6, k_1^- = 1, k_2^- = 11$, the Hamiltonian is

$$H(p, x) = (6x^2 + 6)(e^p - 1) + (x^3 + 11x)(e^{-p} - 1), \tag{4.3}$$

and its convex conjugate, Lagrangian, is

$$\begin{aligned} L(s, x) &= sp^* - H(p^*, x) \\ &= ((6x^2 + 6)e^{p^*} - (x^3 + 11x)e^{-p^*})p^* \\ &\quad - [(6x^2 + 6)(e^{p^*} - 1) + (x^3 + 11x)(e^{-p^*} - 1)]. \end{aligned} \tag{4.4}$$

According to the Eq. (3.2), the optimal curve satisfies the system of ordinary differential equations

$$\begin{aligned} \dot{x} &= (6x^2 + 6)e^p - (x^3 + 11x)e^{-p}, \\ \dot{p} &= -12x(e^p - 1) - (3x^2 + 11)(e^{-p} - 1). \end{aligned} \tag{4.5}$$

According to the Maupertuis principle (3.7), the least action connecting x^A and y with an infinite-time horizon is

$$\begin{aligned} J(y; x^A, c_H) &= \int_0^{T^*} \left((6|x^*|^2 + 6)e^{p^*} - (|x^*|^3 + 11|x^*|)e^{-p^*} \right) p^* \\ &\quad - \left[(6|x^*|^2 + 6)(e^{p^*} - 1) + (|x^*|^3 + 11|x^*|)(e^{-p^*} - 1) \right] dt. \end{aligned} \tag{4.6}$$

Here we omit the argument t in $x^*(t), p^*(t)$.

For Langevin dynamics, consider

$$\nabla U(x) = (x - 1)(x - 2)(x - 3) = -(6x^2 + 6) + (x^3 + 11x). \tag{4.7}$$

We will see later the similarities of the new energy landscape to the chemical reaction (4.5).

The Hamiltonian under the new energy landscape is

$$H(p, x) = p(p - (x - 1)(x - 2)(x - 3)). \tag{4.8}$$

According to the Eq. (3.2), the optimal curve satisfies the system of ordinary differential equations

$$\begin{aligned} \dot{x} &= 2p - (x - 1)(x - 2)(x - 3), \\ \dot{p} &= p(3x^2 - 12x + 11). \end{aligned} \tag{4.9}$$

We cook up this example for Langevin dynamics because when $p = 0$, $\partial_p H(0, x)$ for chemical reaction (4.5) and for (4.9) are exactly same. Then we refer the (4.9) as the diffusion approximation for chemical reaction (4.5). Particularly, they are exactly same at $p = 0$.

Fig. 11 provides an overview of the Hamilton dynamics (4.9) for Langevin dynamics and the chemical reaction (4.5). The first plot illustrates the phase portrait for Langevin dynamics, while the second to fourth plots depict the chemical reaction. Moreover, the third and fourth graphs zoom in on the local periodic orbits shown in the second graph. To give a comprehensive view of the directional field, multiple trajectories are included and distinguished by different colors. The starting point is marked blue, and the ending point is marked red. A trajectory with no blue dot or red dot is periodic. By examining these graphs, one can observe that both Langevin dynamics and the chemical reaction possess periodic orbits, with the latter having much smaller size compared to the former.

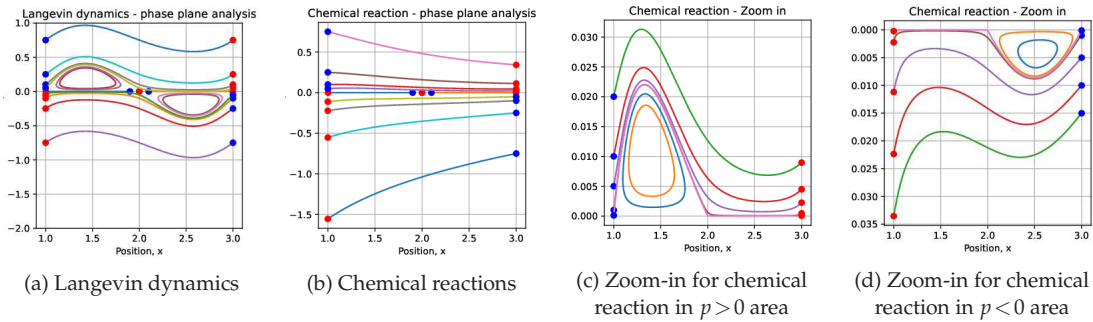


Figure 11: Langevin dynamics and chemical reactions: overview of phase planes. The first plot displays Langevin dynamics (4.9), while the second to fourth plots exhibit the chemical reaction (4.5). The third and fourth graphs zoom in on local periodic orbits in the second graph. The trajectories are colored differently. Comparing the two systems, one may notice that both possess periodic orbits, with the chemical reaction having smaller orbits than Langevin dynamics.

4.2 Comparisons for basic properties: Symmetry, stability, and downhill zero cost path

We first give the following abstract lemma on the gradient flow structure implied via the symmetry of Hamiltonian. Then we show basic properties including symmetry, stability, and downhill zero cost paths.

Lemma 4.1. *Let $H(p,x)$ be a Hamiltonian convex with respect to p and satisfying $H(0,x) \equiv 0$. Assume there exists a function $\psi(x)$ such that one has symmetric property*

$$H(\nabla\psi(x) - p, x) = H(p, x).$$

Then we have the gradient flow structure for the zero-cost flow (2.27)

$$\frac{dx}{dt} = \partial_p H(0, x) = -K(x) \nabla\psi(x), \tag{4.10}$$

where

$$K(x) = \int_0^1 \frac{1}{2} \nabla_{pp}^2 H(\theta\psi(x), x) d\theta.$$

This lemma was proved in [14, Proposition 4.4]. We remark that the relation between the symmetry of the Hamiltonian and the gradient flow structure was studied [22, 26, 29] in more general contexts which includes the generalized gradient flows.

For chemical reaction (4.5), one can directly verify that

$$\psi(x) = \int_{x^A}^x \log\left(\frac{s^3 + 11s}{6s^2 + 2}\right) ds$$

is a stationary solution to the HJE $H(\nabla\psi(x), x) = 0$.

The following lemmas summarize the basic properties of the Hamilton dynamics (4.9) for Langevin dynamics and chemical reaction (4.5). The proofs of these lemmas can be found in the appendix.

Lemma 4.2. *Hamiltonian for Langevin dynamics (4.8) exhibits symmetry with respect to the point $(2, 0)$; moreover, Hamiltonian (4.8) exhibits symmetry with respect to $\nabla U(x)/2$, i.e.,*

$$(i) \quad H(-x+2, -p) = H(x+2, p),$$

$$(ii) \quad H(\nabla U(x) - p, x) = H(p, x).$$

Hamiltonian for chemical reaction (4.3) exhibits symmetry with respect to $\nabla\psi(x)/2$, i.e.,

$$(i) \quad H(\nabla\psi(x) - p, x) = H(p, x).$$

From the symmetry property in the above lemma, we show that both U and V serve as Lyapunov functions and we have two gradient flow structures based on them.

Corollary 4.1. *Both ψ and U are Lyapunov functions for chemical reaction (2.2)*

$$\frac{dU(x)}{dt} = -|\nabla U(x)|^2 \leq 0, \quad (4.11)$$

$$\frac{d\psi(x)}{dt} = -\langle K(x)\nabla\psi(x), \psi(x) \rangle \leq 0. \quad (4.12)$$

In the next section, we will see only ψ can be used to compute the energy barriers associated with the transition path in chemical reactions.

Lemma 4.3. *The Hamilton dynamics (4.9) for Langevin dynamics has five steady points $(1,0), (2,0), (3,0), (2 + \frac{1}{\sqrt{3}}, -\frac{1}{3\sqrt{3}}), (2 - \frac{1}{\sqrt{3}}, \frac{1}{3\sqrt{3}})$. Moreover, the points $(1,0), (2,0), (3,0)$ are saddle points, while $(2 + \frac{1}{\sqrt{3}}, -\frac{1}{3\sqrt{3}})$ and $(2 - \frac{1}{\sqrt{3}}, \frac{1}{3\sqrt{3}})$ are centers.*

Chemical reaction (4.5) has five steady points $(1,0), (2,0), (3,0), (x_1, p_1),$ and $(x_2, p_2),$ where $p_1 < 0$ and $p_2 > 0$. Furthermore, the points $(1,0), (2,0), (3,0)$ are saddle points, while $(x_1, p_1),$ and (x_2, p_2) are centers.

As the proposition for Langevin dynamics has already been proven in the previous section, there is no need to duplicate the proof here.

Proposition 4.1. *Consider the Hamilton dynamics (4.5) for chemical reaction. If there exists a downhill path connecting x^A and y such that Hamiltonian $H(p^*(t), x^*(t)) = 0$ for all $t \in (0, T]$, then the action cost along this path is 0.*

Proof. Let $H(p^*(t), x^*(t)) = 0$, one obtains two solutions curves

$$p^* = 0, \quad p^* = \nabla\psi(x^*) = \log\left(\frac{(x^*)^3 + 11x^*}{6(x^*)^2 + 2}\right).$$

We show that the curve

$$p^* = \log\left(\frac{(x^*)^3 + 11x^*}{6(x^*)^2 + 2}\right)$$

is not a downhill path. We plug it into the first equation in (4.5), then we obtain

$$\dot{x}^* = \nabla U(x^*) = -(6(x^*)^2 + 6) + ((x^*)^3 + 11x^*).$$

Multiplying both sides by $\nabla U(x^*)$ and then taking integral with respect to t yield

$$U(x^*(T)) - U(x^*(0)) = \int_0^T |\nabla U(x^*)|^2 dt \geq 0.$$

Therefore, $U(x^*(T)) \geq U(x^*(0))$ implies $p^* = \nabla U(x^*)$ is not a downhill path.

The solution that meets the downhill process is $p^*(t) = 0$ and $x(t) = 0$. Along this curve, the least action connecting x^A and y is $J(y; x^A, T) = 0$. □

For the Hamilton dynamics (4.9) for Langevin dynamics, Fig. 12 displays multiple curves with fixed initial position $x_0 = 2$ and the initial momentum p_0 asymptotically approaching to 0. The first plot shows momentum/position, the second plot shows position/time, the third plot shows momentum/time, and the last graph shows action cost/initial momentum. From these graphs, one may notice as p_0 asymptotically approaches to 0, the action cost also converges to 0.

For chemical reaction (4.5), Fig. 13 plots several curves with fixed initial position $x_0 = 2$ and a decreasing initial momentum p_0 . The four plots respectively show the relationship between momentum and position, position and time, momentum and time, and action cost and initial momentum. One may observe that as p_0 approaches 0, the action cost also approaches 0.

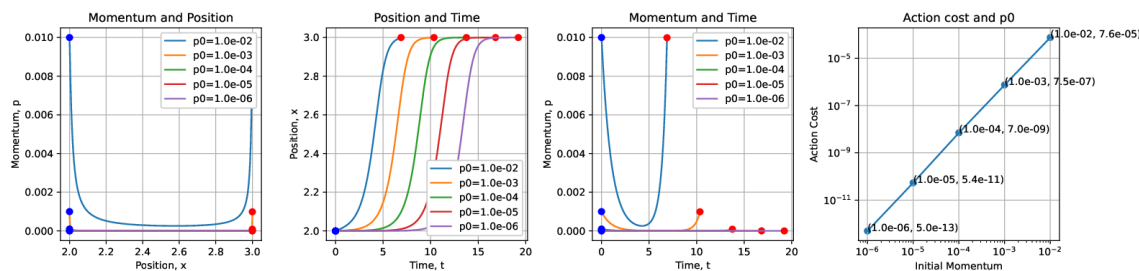


Figure 12: Langevin dynamics: Phase plane for downhill process and corresponding action cost. These plots depict the behavior of (4.9). The first three plots show the relationships between momentum/position, position/time, and momentum/time, respectively. The last plot shows the relationship between action and initial momentum. It can be observed that the reaching time increases monotonically as the initial momentum decreases. Additionally, as the initial momentum p_0 approaches 0, the cost of action converges to 0.

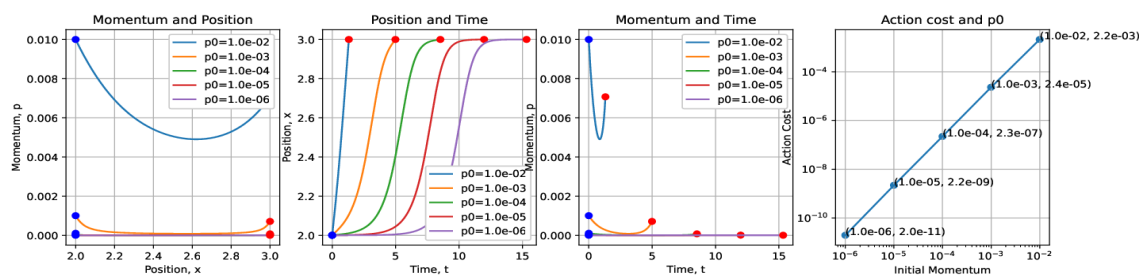


Figure 13: Chemical reactions: Phase plane for downhill process and corresponding action cost. The first three plots are phase portrait for (4.5). These plots refer to chemical reaction (4.5). From these graphs, one may notice that the reaching time monotonically increases the initial momentum approaches to 0. Moreover, the action cost converges to 0.

4.3 Comparisons for uphill transition paths and rates

In this section, we compute the explicit formula for the uphill action cost and compare the energy barriers for the same transition path in a chemical reaction and its diffusion approximation. Then we work out details for the Schlögl catalysis model and its diffusion approximation with illustrative numerical simulations for the uphill transition paths and the associated cost (the minimum energy barrier for transition to happen).

4.3.1 The least action cost: Chemical reaction v.s. diffusion approximation

We first give the following theorem for an abstract Hamiltonian, which use the associated stationary solution to HJE to compute the transition paths and its minimal cost.

Theorem 4.1 (The Implications of Stationary Solution to HJE). *Let $H(p, x)$ be a Hamiltonian convex with respect to p and satisfying $H(0, x) \equiv 0$. Let $\psi(x)$ be the maximal Lipschitz viscosity solution to HJE*

$$H(\nabla\psi(x), x) = 0, \quad \psi(x^A) = 0, \quad (4.13)$$

where x^A is a critical point of $\partial_p H(0, x) = 0$. Then we have

(i) $\psi(x)$ is a Lyapunov function of the zero-cost ODE (2.27) and

$$\frac{d}{dt}\psi(x(t)) = \nabla\psi(x(t)) \cdot \dot{x} = -K(x)\nabla\psi(x) \cdot \nabla\psi(x) \leq 0, \quad (4.14)$$

where

$$K(x) := \int_0^1 (1-\theta)\partial_{pp}H(\theta\nabla\psi(x), x) d\theta.$$

(ii) The uphill least action cost starting from x_i to \bar{x} is given by $\psi(\bar{x})$ and the associated control variable in the Hamilton dynamics (3.8) is $p^*(t) = \nabla\psi(x^*(t))$. That is to say, through $\psi(x)$, we find a Lagrangian graph for the uphill least action path.

Remark 4.1. If $\psi(x^A)$ is not zero, one can subtract a constant because $\psi(x)$ up to a constant, $\psi+c$ is still a stationary solution. We also point out that the above statements do not require a symmetry in Hamiltonian.

Proof of Theorem 4.1. First, notice $H(\nabla\psi(x), x) = 0 = H(0, x)$. We do the Taylor expansion at $p=0$ and obtain

$$\begin{aligned} 0 &= H(\nabla\psi(x), x) \\ &= H(0, x) + \partial_p H(0, x) \cdot \nabla\psi(x) + \int_0^1 (1-\theta)\partial_{pp}H(\theta\nabla\psi(x), x) d\theta \nabla\psi(x) \cdot \nabla\psi(x) \\ &= \dot{x} \cdot \nabla\psi(x) + K(x)\nabla\psi(x) \cdot \nabla\psi(x). \end{aligned}$$

Here

$$K(x) = \int_0^1 (1-\theta)\partial_{pp}H(\theta\nabla\psi(x), x) d\theta$$

is positive definite matrix-valued function due to H is strictly convex in p . Thus we obtain (4.14) and ψ is a Lyapunov function of the zero-cost ODE (2.27).

Second, notice the critical energy level $c_H = 0$ because $L(s, x) \geq 0$ and equals zero if and only if $s = \partial_p H(0, x)$. Then it is well known that the least action cost $V(x; x^A, 0)$ satisfies the stationary HJE (4.13) in the viscosity sense. On the one hand, this least action cost $V(x; x^A, 0)$ is achieved via the Hamiltonian dynamics (3.8), i.e.

$$V(x; x^A, 0) = \inf_{\substack{T > 0, \\ \gamma(0) = x^A, \gamma(T) = x}} \int_0^T L(\dot{\gamma}(t), \gamma(t)) dt.$$

On the other hand, any viscosity solutions u to stationary HJE (4.13) satisfies that for any absolutely continuous curve $\gamma(\cdot)$,

$$\begin{aligned} u(x) - u(x^A) &= \int_0^T \nabla u(\gamma(s)) \cdot \dot{\gamma}(s) ds \\ &\leq \int_0^T \left(L(\dot{\gamma}(s), \gamma(s)) + H(\nabla u(\gamma(s)), \gamma(s)) \right) ds \\ &\leq \int_0^T L(\dot{\gamma}(s), \gamma(s)) ds. \end{aligned} \tag{4.15}$$

Here we used the Fenchel-Young's inequality. Thus, taking infimum with respect to γ and T , we see $V(x; x^A, 0)$ is the largest viscosity solution satisfying $V(x^A; x^A) = 0$.

Third, from the definition of Legendre transform, for any curve $\gamma(t)$

$$L(\dot{\gamma}, \gamma) = \sup_p (\dot{\gamma} \cdot p - H(p, \gamma)) \geq \dot{\gamma} \cdot \nabla \psi(\gamma) - H(\nabla \psi(\gamma), \gamma) = \frac{d\psi(\gamma(t))}{dt}, \tag{4.16}$$

where we used ψ is the stationary solution to (4.13). On the other hand, we verified in the second step that the least action is achieved at

$$\psi(x) - \psi(x^A) = \frac{d\psi(\gamma(t))}{dt} = \inf_T \inf_{\substack{\gamma(0) = x^A, \\ \gamma(T) = x}} \int_0^{T^*} L(\dot{\gamma}(t), \gamma(t)) dt. \tag{4.17}$$

Thus the optimal trajectory is given by

$$\dot{\gamma} = \partial_p H(p^*(t), \gamma(t)), \quad p^*(t) = \nabla \psi(\gamma(t)), \tag{4.18}$$

and the last statement in (ii) follows. □

Based on the above proposition for abstract Hamiltonian, we find an explicit formula for the uphill least action cost for chemical reactions.

Proposition 4.2. *For chemical reactions, if $U'(x^A) = 0$, $U''(x^A) \geq 0$ and there are finite critical points $x_1 < x_2 < \dots < x_K$ between x^A and y , we have an explicit uphill action cost formula for least action curve starting from x^A to y*

$$\psi(y; x^A, 0) = \begin{cases} \int_{x^A}^y \log \frac{x^3 + 11x}{6x^2 + 6} dx, & y \in [x^A, x_1], \\ \int_{x^A}^{x_1} \log \frac{x^3 + 11x}{6x^2 + 6} dx, & y \in [x_1, x_2], \\ \int_{x^A}^{x_1} \log \frac{x^3 + 11x}{6x^2 + 6} dx + \int_{x_2}^y \log \frac{x^3 + 11x}{6x^2 + 6} dx, & y \in [x_2, x_3], \\ \dots & \end{cases} \quad (4.19)$$

Proof. First, notice that starting from any critical point x_k of U , $\psi(y; x^A, 0)$ is a classical solution to stationary HJE $H(\nabla\psi(y), y) = 0$ in any open interval (x^A, x_1) , (x_k, x_{k+1}) , $k = 1, \dots, K-1$.

Second, at the connection points x_k , $k = 1, \dots, K$, we consider the following two cases:

- (i) If x_i is a local minimum of U , then the left slope of ψ is zero, which coincides with the right slope of ψ .
- (ii) If x_i is a local maximum of U , then the right slope of ψ is zero, which also coincides with the left slope of ψ .

Therefore, $\psi(y; x^A, 0)$ is a viscosity solution to the stationary HJE

$$H(\nabla\psi(y), y) = 0, \quad \psi(x^A) = 0.$$

Third, for the uphill intervals $[x^A, x_1]$ and $[x_{2k}, x_{2k+1}]$, one can directly verify $p^*(y) = \nabla\psi(y)$ solves (4.5) and thus the associated trajectory (4.18) is an uphill least action curve. Similarly, for downhill intervals $[x_{2k-1}, x_{2k}]$, one can also verify $p^*(y) = \nabla\psi(y) = 0$ solves (4.5) and thus a downhill least action curve. From the argument in (4.15), we know $\psi(y; x^A, 0)$ is the maximal Lipschitz viscosity solution and thus from Theorem 4.1(ii), we conclude this proposition. \square

Fig. 14 illustrates the uphill process of the Hamilton dynamics (4.9) for Langevin dynamics. The four plots show the relationships between position/momentum, position/time, momentum/time, and action cost/initial momentum. The

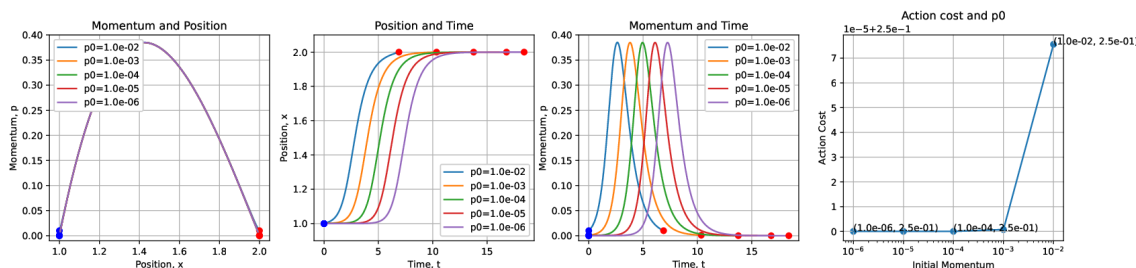


Figure 14: Langevin dynamics: Uphill process and the least action cost. The first three plots are phase portrait for the Hamilton dynamics (4.9) for Langevin dynamics with fixed initial position $x_0=1$ and varying initial momentum p_0 . From these graphs, one may notice the action cost monotonically decreases with the decrease of initial momentum p_0 . As the initial momentum p_0 approaches to 0, the action cost converges to a positive value of approximately 0.25.

plots include five curves with initial momenta approaching to 0, while the initial and terminal positions remain fixed as $x_0=1$ and $x=2$, respectively. The results reveal that as the initial momentum p_0 approaches 0, the required terminal time approaches infinity, and the action converges to a positive value of approximately 0.25.

Fig. 15 displays the uphill process of chemical reaction (4.5). The four plots show that the relationships between position/momentum, position/time, momentum/time, and action cost/initial momentum. The plots feature five curves with initial momenta approaching 0, while the initial and terminal positions remain fixed at $x_0 = 1$ and $x = 2$, respectively. As the initial momentum p_0 approaches 0, the required terminal time approaches infinity, and the action converges to a positive value of approximately 0.0135.

These plots provide evidence that the least action connecting $x = 1$ and $x = 2$ relates to the size enclosed by the downhill/uphill least action curves. We sum-

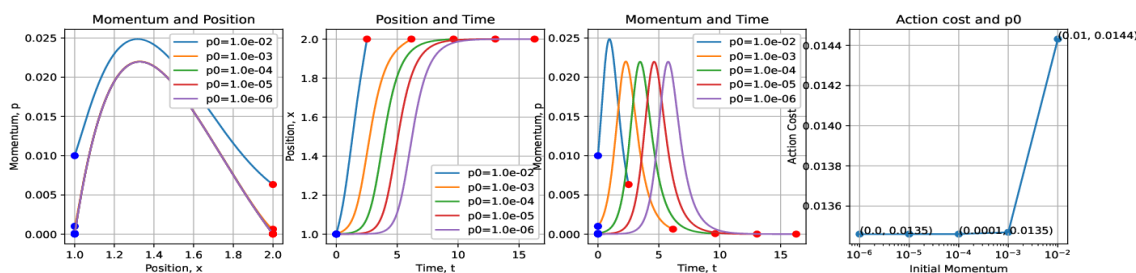


Figure 15: Chemical reactions: Uphill process and the least action cost. The first three plots are phase portrait for chemical reactions (4.5) with fixed initial position $x_0=1$ and varying initial momentum p_0 . From these graphs, one may notice the action cost monotonically increases with the initial momentum p_0 . Specifically, as the initial momentum p_0 approaches to 0, the action cost converges to approximately 0.0135.

marize it as the following proposition.

Proposition 4.3. *Under the assumption of Theorem 4.1, assume further x^A is a local minimum of U and x_1 is the local maximum of U near by x^A . On the phase plane xp -plane, denote by A the area enclosed by the downhill least action trajectory connecting x_1 to x^A and the uphill least action trajectory connecting x^A to x_1 . Then we have*

(i) *The area for the diffusion approximation is*

$$A = \int_{x^A}^{x_1} \nabla U(x) dx = U(x_1) - U(x^A).$$

(ii) *The area for the original chemical reaction is*

$$A = \int_{x^A}^{x_1} \nabla \psi(x) dx = \psi(x_1) - \psi(x^A),$$

where

$$\psi(x) = \int_{x^A}^x \log \left(\frac{s^3 + 11s}{6s^2 + 2} \right) ds.$$

Proof. From Theorem 4.1(ii), we know the uphill least action curve is given by the Lagrangian graph $p^* = \nabla \psi(x^*)$. Then the area enclosed by $p(x) = 0$ and $p(x) = \nabla \psi(x)$ is just $\int_{x^A}^{x_1} \nabla \psi(x) dx$. That is to say, we just need to find the maximal Lipschitz stationary solution to $H(\nabla \psi(x), x) = 0$ with $\psi(x^A) = 0$. As we proved before, $U(x)$ and

$$\psi(x) = \int_{x^A}^x \log \left(\frac{s^3 + 11s}{6s^2 + 2} \right) ds$$

for $x \in [x^A, x_1]$ do the job. □

For Hamiltonian of Langevin dynamics (4.8), letting $H(p^*(t), x^*(t)) = 0$ yields two curves: $p^*(t) = x^*(t) = 0$ and $p^*(x^*) = (x^* - 1)(x^* - 2)(x^* - 3)$. The area enclosed by the two curves connecting $x = 1$ and $x = 2$ in the second quadrant is

$$\int_1^2 (x-1)(x-2)(x-3) dx = 0.25. \quad (4.20)$$

For Hamiltonian of chemical reaction (4.3), the computation is similar. The enclosed area by curves connecting $x = 1$ and $x = 2$ with $H(p^*(t), x^*(t)) = 0$ is 0.01346 in approximation. Moreover, the least action connecting $x = 1$ and $x = 2$ is

$$V(2;1,0) = \int_1^2 \log \frac{x^3 + 11x}{6x^2 + 6} dx \approx 0.01346.$$

Indeed, the values of area match the least action connecting $x = 1$ and $x = 2$.

4.3.2 The transition rate: chemical reaction v.s. diffusion approximation

In this subsection, we illustrate the transition rate for a chemical reaction by using the example. For the same transition path connection two critical points of U in the diffusion approximation and ψ in the chemical reaction, we compare their transition rates in the following definition.

Definition 4.1. Given a curve $(x(t), p(t))$ of a dynamical system, suppose the arrival time of two points (x_1, p_1) and (x_2, p_2) are t_1 and t_2 , respectively. The transition rate between (x_1, p_1) and (x_2, p_2) is $1/(t_2 - t_1)$.

Fig. 16 compares the transition rate for two dynamics. The dashed line refers to the Hamilton dynamics (4.9) for Langevin dynamics, and the solid line refers to the chemical reaction (4.5). The first plot sketches four curves with selected initial conditions, in order to provide an overview. The second plot specifically compares the uphill process of two dynamics with momentum/position relation. The third plot shows the momentum/time relation. The last plot compares the action cost with respect to the initial momenta.

Consider the transition rate between $x = 1$ and $x = 2$. With fixed initial momentum $p_0 = 0$, the transition rate is 0. With fixed initial momentum $p_0 > 0$, the transition rates for two dynamics generally do not match. However, from the third plot, one may notice that as the initial momentum p_0 asymptotically approaches to 0, the transition rates go to infinity with closer and closer difference. Last but not the least, the least action differ by more than ten times: Langevin dynamics has least action cost 0.25, while the chemical reaction has only 0.01346.

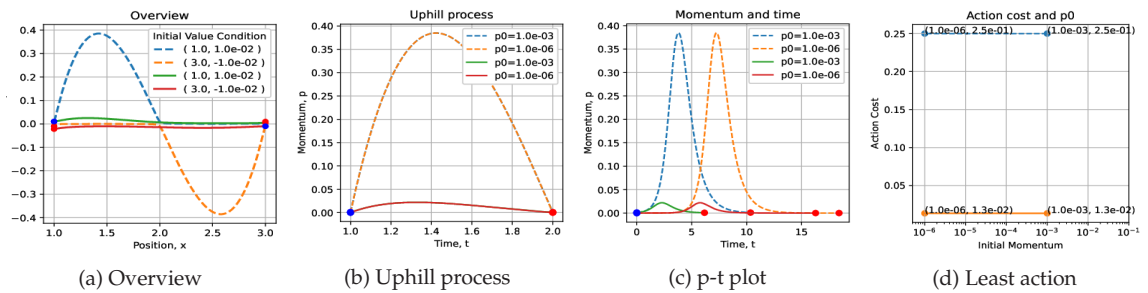


Figure 16: Langevin and chemical reaction: Transition rate comparison. The dashed line represents Langevin dynamics (4.9), and the solid line represents chemical reaction (4.5). The first plot shows four curves with different initial conditions, and the second and third plots compare the momentum/position and momentum/time relationships for the uphill process of the two dynamics, respectively. The last plot compares the action cost with respect to the initial momentum. It can be observed that the transition rate of the two dynamics do not match whenever the $p_0 > 0$. Nevertheless, as the initial momentum p_0 approaches 0, they get closer. Additionally, the least action cost differs by more than ten times, with Langevin dynamics having a least action cost of 0.25, while chemical reaction has only 0.01346.

It provides an evidence that the diffusion process in the uphill process accurately approximate the transition rates. However, the approximation is not accurate with respect to the least action cost.

5 Conclusion

The mathematical structures and quantitative properties for non-equilibrium chemical reactions are important and challenging questions because the structures are not symmetric, not convex, and irreversible. We focus on exploring the Hamilton structure in chemical reactions and its implications. We first compare the Maupertuis principle and the Hamilton principle for the least action problem associated with the Hamiltonian for classical mechanics and Langevin dynamics. This leads to the conclusion that one should use the Maupertuis principle with an undefined terminal time for computing transition paths in chemical reactions. We then study quantitative properties for the downhill/uphill transition paths in chemical reactions and its diffusion approximation. Based on the Hamilton-Jacobi method, we first find the selected stationary solution $\psi(x)$ to the limiting HJE, which can be used to construct an exact barrier function $p^*(x) = \nabla\psi(x^*)$ in the transition path calculations. Our numerical simulations based on the Hamilton dynamics also verify this exact formula for computing the energy barrier and related it to the geometric interpretations in the phase plane. Using the one-dimensional example, we show the transition rates get closer when the initial momentum asymptotically approach to zero, while the transition path in the diffusion approximation undergoes more significantly in size. Selecting stationary solution to the limiting HJE plays an important role for computing the global energy landscape. Although numerical experiments show the selected stationary solution captures all the asymptotic behaviors for the original non-equilibrium chemical reaction, whether this stationary solution is the rate function for the large deviation principle of the invariant measures for non-equilibrium chemical reactions is still an open question.

Appendix A. Some elementary proofs for symmetry and stability

In this section, we give some elementary proofs for completeness.

Proof for Lemma 3.1. For classical mechanics, to show $H(-p, x) = H(p, x)$, one may

perform some elementary computations

$$H(-p, x) = \frac{|-p|^2}{2} + U(x) = \frac{|p|^2}{2} + U(x) = H(p, x). \quad (\text{A.1})$$

To show $H(p, -x) = H(p, x)$, we can similarly show

$$H(p, -x) = \frac{|p|^2}{2} + U(-x) = \frac{|p|^2}{2} + U(x) = H(p, x). \quad (\text{A.2})$$

To prove $H(-p, -x) = H(p, x)$, we can similarly show

$$H(-p, -x) = \frac{|-p|^2}{2} + U(-x) = \frac{|p|^2}{2} + U(x) = H(p, x). \quad (\text{A.3})$$

For Langevin dynamics, to show $H(-p, -x) = H(p, x)$, we can show

$$H(-p, -x) = (-p)(-p - 4x + 4x^3) = p(p + 4x - 4x^3) = H(p, x). \quad (\text{A.4})$$

Similarly,

$$\begin{aligned} H(\nabla U(x) - p, x) &= (\nabla U(x) - p)(\nabla U(x) - p - \nabla U(x)) \\ &= p(p - \nabla U(x)) = H(p, x). \end{aligned} \quad (\text{A.5})$$

The proof is complete. \square

Proof for Lemma 3.2. The Hamiltonian evaluated at the initial point (x_0, p_0) is

$$H_0 = \frac{1}{2}p_0^2 + (x_0^2 - 1)^2. \quad (\text{A.6})$$

Along the curve that meets the initial condition (x_0, p_0) , Hamiltonian preserves as a constant

$$\frac{1}{2}(p(t))^2 + ((x(t))^2 - 1)^2 = H_0, \quad \forall t. \quad (\text{A.7})$$

Then we may parametrize the Hamiltonian above with trigonometric functions

$$p = \sqrt{2H_0} \cos(\omega t), \quad x^2 = \sqrt{H_0} \sin(\omega t) + 1. \quad (\text{A.8})$$

The parameter ω implicitly depends on H_0 , or equivalently x_0 and p_0 . The parametrization shows any orbit is periodic.

Suppose the initial condition is $(x_0, 0)$, where $x_0 \in (0, 1)$. The parametrized formula shows the maximum position that the trajectory can reach is $x_{\max} = \sqrt{2 - x_0^2}$. Since the trajectory is symmetric with respect to x axis, one may derive the period formula from the equation $dt = dx/p$

$$T = 2 \int_{x_0}^{x_{\max}} \frac{1}{\sqrt{(x_0 - 1)^2 - (x^2 - 1)^2}} dx. \quad (\text{A.9})$$

By trigonometric substitution $\sin(\theta) = (x^2 - 1)/(x_0^2 - 1)$, a simpler form is obtained

$$T = \frac{\sqrt{2}}{2} \int_{\frac{\pi}{2}}^{\frac{3\pi}{2}} \frac{1}{\sqrt{(x_0^2 - 1)\sin(\theta) + 1}} d\theta. \quad (\text{A.10})$$

This formula shows the period T monotonically decreases with $x_0 \in (0, 1)$. Furthermore,

$$\inf_{x_0 \in (0, 1)} T = \frac{\sqrt{2}}{2} \pi.$$

Suppose the initial condition is $(0, p_0)$, where $p_0 \in (0, +\infty)$. The trajectory is symmetric with respect to x and p axis, then the period formula is

$$T = 4 \int_0^{\sqrt{\sqrt{\frac{1}{2}p_0^2 + 1} + 1}} \frac{1}{\sqrt{p_0^2 + 2 - 2(x^2 - 1)^2}} dx. \quad (\text{A.11})$$

Let $a = \sqrt{p_0^2/2 + 1}$ and $\sin(\theta) = (x^2 - 1)/a$. Then, we may obtain a simpler form

$$T = \sqrt{2} \int_{-\arcsin(\frac{1}{a})}^{\frac{\pi}{2}} \frac{1}{\sqrt{1 + a\sin(\theta)}} d\theta. \quad (\text{A.12})$$

The lower limit of the integral and the denominator of the integrand increase with p_0 , so the period monotonically decreases with $p_0 \in (0, \infty)$. \square

Proof for Lemma 3.3. For the classical mechanics dynamics system (3.24), setting $\dot{p} = 0$ and $\dot{x} = 0$ yields three steady points: $(1, 0)$, $(-1, 0)$, and $(0, 0)$. The Jacobi matrix in the point (x, p) is

$$J(x, p) = \begin{pmatrix} 0 & 1 \\ 4 - 12x^2 & 0 \end{pmatrix}. \quad (\text{A.13})$$

First, we diagonalize the Jacobi matrix at $(0,0)$

$$J(0,0) = \begin{pmatrix} 0 & 1 \\ 4 & 0 \end{pmatrix} = \begin{pmatrix} 1 & -1 \\ 2 & 2 \end{pmatrix} \begin{pmatrix} 2 & 0 \\ 0 & -2 \end{pmatrix} \begin{pmatrix} \frac{1}{2} & \frac{1}{4} \\ -\frac{1}{2} & \frac{1}{4} \end{pmatrix}. \tag{A.14}$$

This shows $(0,0)$ is a saddle point.

Then we diagonalize the Jacobi matrix at the point $(\pm 1,0)$

$$J(\pm 1,0) = \begin{pmatrix} 0 & 1 \\ -8 & 0 \end{pmatrix} = \begin{pmatrix} -\sqrt{2}i & \sqrt{2}i \\ 4 & 4 \end{pmatrix} \begin{pmatrix} 2\sqrt{2}i & 0 \\ 0 & -2\sqrt{2}i \end{pmatrix} \begin{pmatrix} i\frac{\sqrt{2}}{4} & \frac{1}{8} \\ -i\frac{\sqrt{2}}{4} & \frac{1}{8} \end{pmatrix}. \tag{A.15}$$

The stability in $(1,0)$ and $(-1,0)$ are either centers or spiral points. Since all solutions in classical mechanics dynamics is periodic, spiral case can be ruled out. Thus, $(1,0)$ and $(-1,0)$ are centers.

For the Hamilton dynamics (3.26) for Langevin dynamics, setting $\dot{p} = 0$ and $\dot{x} = 0$ yields 5 steady points

$$(0,0), (1,0), (-1,0), \left(\frac{1}{\sqrt{3}}, -\frac{4}{3\sqrt{3}}\right), \left(-\frac{1}{\sqrt{3}}, \frac{4}{3\sqrt{3}}\right).$$

The Jacobi matrix at the point (x,p) is

$$J = \begin{pmatrix} -12x^2 + 4 & 2 \\ 24xp & 12x^2 - 4 \end{pmatrix}.$$

First we diagonalize the Jacobi matrix at $(-1,0), (0,0)$, and $(1,0)$.

$$J(-1,0) = J(1,0) = \begin{pmatrix} -8 & 2 \\ 0 & 8 \end{pmatrix} = \begin{pmatrix} 1 & 1 \\ 8 & 0 \end{pmatrix} \begin{pmatrix} 8 & 0 \\ 0 & -8 \end{pmatrix} \begin{pmatrix} 0 & \frac{1}{8} \\ 1 & -\frac{1}{8} \end{pmatrix}, \tag{A.16}$$

$$J(0,0) = \begin{pmatrix} 4 & 2 \\ 0 & -4 \end{pmatrix} = \begin{pmatrix} 1 & -1 \\ 0 & 4 \end{pmatrix} \begin{pmatrix} 4 & 0 \\ 0 & -4 \end{pmatrix} \begin{pmatrix} 1 & \frac{1}{4} \\ 0 & \frac{1}{4} \end{pmatrix}. \tag{A.17}$$

This shows $(-1,0), (0,0)$, and $(1,0)$ are saddle points.

Then, we diagonalize the Jacobi matrix at $(-\frac{1}{\sqrt{3}}, \frac{4}{3\sqrt{3}})$ and $(\frac{1}{\sqrt{3}}, -\frac{4}{3\sqrt{3}})$

$$\begin{aligned} J\left(-\frac{1}{\sqrt{3}}, \frac{4}{3\sqrt{3}}\right) &= J\left(\frac{1}{\sqrt{3}}, -\frac{4}{3\sqrt{3}}\right) = \begin{pmatrix} 0 & 2 \\ -8 & 0 \end{pmatrix} \\ &= \begin{pmatrix} -i & i \\ 2 & 2 \end{pmatrix} \begin{pmatrix} 4i & 0 \\ 0 & -4i \end{pmatrix} \begin{pmatrix} i\frac{1}{2} & \frac{1}{4} \\ -i\frac{1}{2} & \frac{1}{4} \end{pmatrix}. \end{aligned} \tag{A.18}$$

This shows $(-\frac{1}{\sqrt{3}}, \frac{4}{3\sqrt{3}})$ and $(\frac{1}{\sqrt{3}}, -\frac{4}{3\sqrt{3}})$ are either centers or spiral points. Further investigation requires computing Hessian matrix. For the Hamiltonian (3.25), the Hessian matrix at point (x, p) is

$$(\text{Hess } H)(x, p) = \begin{pmatrix} -24xp & 4 - 12x^2 \\ 4 - 12x^2 & 2 \end{pmatrix}. \quad (\text{A.19})$$

Then, we diagonalize the Hessian matrix at $(-\frac{1}{\sqrt{3}}, \frac{4}{3\sqrt{3}})$ and $(\frac{1}{\sqrt{3}}, -\frac{4}{3\sqrt{3}})$

$$(\text{Hess } H)\left(-\frac{1}{\sqrt{3}}, \frac{4}{3\sqrt{3}}\right) = (\text{Hess } H)\left(\frac{1}{\sqrt{3}}, -\frac{4}{3\sqrt{3}}\right) = \begin{pmatrix} \frac{24}{3} & 0 \\ 0 & 2 \end{pmatrix}. \quad (\text{A.20})$$

All eigenvalues of the Hessian matrix in the two steady states are positive. Therefore, two steady points are the local minimum. In a Hamilton dynamics, each curve will not change its level, so we may safely rule out the spiral case and conclude that $(-\frac{1}{\sqrt{3}}, \frac{4}{3\sqrt{3}}), (\frac{1}{\sqrt{3}}, -\frac{4}{3\sqrt{3}})$ are centers. \square

Proof for Lemma 4.2. For Hamilton dynamics (4.8) for Langevin dynamics, recall (2.14). We have $b(x) = -\nabla U(x)$. Then, $b(x)$ is symmetric with respect to the point $(2, 0)$, i.e., $b(2-x) = -b(2+x)$ for all x . Shifting the system two units to the left, one may derive $H(x+2, p) = p(p+b(x+2))$. Substituting x and p with $-x$ and $-p$, respectively, one may derive

$$H(-p, -x+2) = -p(-p+b(-x+2)) = p(p+b(x+2)) = H(p, x+2). \quad (\text{A.21})$$

It shows the shifted system is symmetric with respect to the origin. Therefore, the original system is symmetric with respect to $(2, 0)$. Similarly,

$$\begin{aligned} H(\nabla U(x) - p, x) &= (\nabla U(x) - p)(\nabla U(x) - p - \nabla U(x)) \\ &= p(p - \nabla U(x)) = H(p, x). \end{aligned} \quad (\text{A.22})$$

For Hamiltonian of chemical reaction (4.3), we perform the following computation:

$$\begin{aligned} H(\nabla \psi(x) - p, x) &= (6x^2 + 6)(e^{\nabla \psi - p} - 1) + (x^3 + 11x)(e^{p - \nabla \psi} - 1) \\ &= (6x^2 + 6)\left(\frac{x^3 + 11x}{6x^2 + 6}e^{-p} - 1\right) + (x^3 + 11x)\left(e^p \frac{6x^2 + 6}{x^3 + 11x} - 1\right) \\ &= (x^3 + 11x)e^{-p} - (6x^2 + 6) + e^p(6x^2 + 6) - (x^3 + 11x) \\ &= (6x^2 + 6)(e^p - 1) + (x^3 + 11x)(e^{-p} - 1) \\ &= H(p, x). \end{aligned}$$

The proof is complete. \square

Proof for Lemma 4.3. For Hamilton dynamics (4.9) Langevin dynamics, setting $\dot{p} = 0$ and $\dot{x} = 0$ yields 5 steady points

$$(1,0), (2,0), (3,0), \left(2 + \frac{1}{\sqrt{3}}, -\frac{1}{3\sqrt{3}}\right), \left(2 - \frac{1}{\sqrt{3}}, \frac{1}{3\sqrt{3}}\right).$$

The Jacobi matrix in the point (x,p) is

$$J(x,p) = \begin{pmatrix} -3x^2 + 12x - 11 & 2 \\ p(6x - 12) & 3x^2 - 12x + 11 \end{pmatrix}.$$

First we diagonalize the Jacobi matrix at $(1,0), (2,0)$, and $(3,0)$

$$J(1,0) = J(3,0) = \begin{pmatrix} -2 & 2 \\ 0 & 2 \end{pmatrix} = \begin{pmatrix} 1 & 1 \\ 2 & 0 \end{pmatrix} \begin{pmatrix} 2 & 0 \\ 0 & -2 \end{pmatrix} \begin{pmatrix} 0 & \frac{1}{2} \\ 1 & -\frac{1}{2} \end{pmatrix}, \tag{A.23}$$

$$J(2,0) = \begin{pmatrix} 1 & 2 \\ 0 & -1 \end{pmatrix} = \begin{pmatrix} 1 & -1 \\ 0 & 1 \end{pmatrix} \begin{pmatrix} 1 & 0 \\ 0 & -1 \end{pmatrix} \begin{pmatrix} 1 & 1 \\ 0 & 1 \end{pmatrix}. \tag{A.24}$$

It shows $(1,0), (2,0), (3,0)$ are saddle points.

Then, we diagonalize the Jacobi matrix at $(2 + \frac{1}{\sqrt{3}}, -\frac{1}{3\sqrt{3}})$, and $(2 - \frac{1}{\sqrt{3}}, \frac{1}{3\sqrt{3}})$

$$\begin{aligned} J\left(2 + \frac{1}{\sqrt{3}}, -\frac{1}{3\sqrt{3}}\right) &= J\left(2 - \frac{1}{\sqrt{3}}, \frac{1}{3\sqrt{3}}\right) = \begin{pmatrix} 0 & 2 \\ -\frac{2}{3} & 0 \end{pmatrix} \\ &= \begin{pmatrix} -\sqrt{3}i & \sqrt{3}i \\ 1 & 1 \end{pmatrix} \begin{pmatrix} \frac{2}{\sqrt{3}}i & 0 \\ 0 & -\frac{2}{\sqrt{3}}i \end{pmatrix} \begin{pmatrix} i\frac{\sqrt{3}}{6} & \frac{1}{2} \\ -i\frac{\sqrt{3}}{6} & \frac{1}{2} \end{pmatrix}. \end{aligned} \tag{A.25}$$

It shows $(2 + \frac{1}{\sqrt{3}}, -\frac{1}{3\sqrt{3}})$, and $(2 - \frac{1}{\sqrt{3}}, \frac{1}{3\sqrt{3}})$ are either centers or spiral points. Further investigation requires computing Hessian matrix. For the Hamiltonian (4.8), the Hessian matrix at point (x,p) is

$$(\text{Hess } H)(x,p) = \begin{pmatrix} 2 & -3x^2 + 12x - 11 \\ -3x^2 + 12x - 11 & -6p(x-2) \end{pmatrix}. \tag{A.26}$$

Then, we diagonalize the Hessian matrix at $(2 + \frac{1}{\sqrt{3}}, -\frac{1}{3\sqrt{3}})$ and $(2 - \frac{1}{\sqrt{3}}, \frac{1}{3\sqrt{3}})$

$$(\text{Hess } H)\left(2 + \frac{1}{\sqrt{3}}, -\frac{1}{3\sqrt{3}}\right) = (\text{Hess } H)\left(2 - \frac{1}{\sqrt{3}}, \frac{1}{3\sqrt{3}}\right) = \begin{pmatrix} 2 & 0 \\ 0 & \frac{2}{3} \end{pmatrix}. \tag{A.27}$$

All eigenvalues of the Hessian matrix in the two steady states are positive. Therefore, two steady points are the local minimum. In a Hamilton dynamics, each

curve will not change its level, so we may safely rule out the spiral case and conclude that $(2 + \frac{1}{\sqrt{3}}, -\frac{1}{3\sqrt{3}})$ and $(2 - \frac{1}{\sqrt{3}}, \frac{1}{3\sqrt{3}})$ are centers.

For chemical reaction (4.5), setting $\dot{p}=0$, $\dot{x}=0$, and $p=0$ yields 3 steady points: $(1,0), (2,0), (3,0)$. The Jacobi matrix is

$$J(x,p) = \begin{pmatrix} 12xe^p - (3x^2+11)e^{-p} & (6x^2+6)e^p + (x^3+11x)e^{-p} \\ -12(e^p-1) - 6x(e^{-p}-1) & -12xe^p + (3x^2+11)e^{-p} \end{pmatrix}.$$

We diagonalize the Jacobi matrix at $(1,0), (2,0), (3,0)$

$$J(1,0) = \begin{pmatrix} -2 & 24 \\ 0 & 2 \end{pmatrix} = \begin{pmatrix} 6 & 1 \\ 1 & 0 \end{pmatrix} \begin{pmatrix} 2 & 0 \\ 0 & -2 \end{pmatrix} \begin{pmatrix} 0 & 1 \\ 1 & -6 \end{pmatrix}, \quad (\text{A.28})$$

$$J(2,0) = \begin{pmatrix} 1 & 60 \\ 0 & -1 \end{pmatrix} = \begin{pmatrix} 1 & -30 \\ 0 & 1 \end{pmatrix} \begin{pmatrix} 1 & 0 \\ 0 & -1 \end{pmatrix} \begin{pmatrix} 1 & 30 \\ 0 & 1 \end{pmatrix}, \quad (\text{A.29})$$

$$J(3,0) = \begin{pmatrix} -2 & 120 \\ 0 & 2 \end{pmatrix} = \begin{pmatrix} 30 & 1 \\ 1 & 0 \end{pmatrix} \begin{pmatrix} 2 & 0 \\ 0 & -2 \end{pmatrix} \begin{pmatrix} 0 & 1 \\ 1 & -30 \end{pmatrix}. \quad (\text{A.30})$$

This shows $(1,0), (2,0), (3,0)$ are saddle points.

Note that $\det(J(x_1, p_1)) > 0$ and $\det(J(x_2, p_2)) > 0$. Therefore, the characteristic equation of Jacobi matrix in (x_1, y_1) and (x_2, y_2) has two purely imaginary roots. Thus, (x_1, y_1) and (x_2, y_2) are either centers or spiral points. With similar process to compute the Hessian matrix, we may conclude the two points are centers. \square

Acknowledgments

The authors would like to thank the undergraduate research program VIP at Purdue. Yuan Gao was supported by NSF under Award DMS-2204288.

References

- [1] D. F. Anderson and T. G. Kurtz, *Stochastic Analysis of Biochemical Systems*, Springer, 2015.
- [2] L. Bertini, A. De Sole, D. Gabrielli, G. Jona-Lasinio, and C. Landim, *Macroscopic fluctuation theory*, Rev. Modern Phys. 87(2) (2015), 593–636.
- [3] W. Bryc, *Large deviations by the asymptotic value method*, in: *Diffusion Process and Related Problems in Analysis, Vol. I. Diffusions in Analysis and Geometry*, Birkhäuser, 1990, 447–472.

- [4] G. Contreras, *Action potential and weak KAM solutions*, Calc. Var. Partial Differential Equations 13(4) (2001), 427–458.
- [5] C. R. Doering, K. V. Sargsyan, and L. M. Sander, *Extinction times for birth-death processes: Exact results, continuum asymptotics, and the failure of the Fokker-Planck approximation*, Multiscale Model. Simul. 3(2) (2005), 283–299.
- [6] M. I. Dykman, E. Mori, J. Ross, and P. M. Hunt, *Large fluctuations and optimal paths in chemical kinetics*, J. Chem. Phys. 100(8) (1994), 5735–5750.
- [7] W. E, W. Ren, and E. Vanden-Eijnden, *String method for the study of rare events*, Phys. Rev. B 66(5) (2002), 052301.
- [8] W. E, W. Ren, and E. Vanden-Eijnden, *Minimum action method for the study of rare events*, Comm. Pure Appl. Math. 57(5) (2004), 637–656.
- [9] W. E and E. Vanden-Eijnden, *Towards a theory of transition paths*, J. Stat. Phys. 123(3) (2006), 503–523.
- [10] M. Esposito, *Open questions on nonequilibrium thermodynamics of chemical reaction networks*, Commun. Chem. 3(1) (2020), 1–3.
- [11] M. Feinberg, *Foundations of Chemical Reaction Network Theory*, in: *Applied Mathematical Sciences*, Vol. 202, Springer, 2019.
- [12] H. Gang, *Stationary solution of master equations in the large-system-size limit*, Physical Review A 36(12) (1987), 5782–5790.
- [13] Y. Gao, T. Li, X. Li, and J.-G. Liu, *Transition path theory for Langevin dynamics on manifolds: Optimal control and data-driven solver*, Multiscale Model. Simul. 21 (2023), 1–33.
- [14] Y. Gao and J.-G. Liu, *Revisit of macroscopic dynamics for some non-equilibrium chemical reactions from a Hamiltonian viewpoint*, J. Stat. Phys. 189(2) (2022), 1–57.
- [15] Y. Gao and J.-G. Liu, *A selection principle for weak KAM solutions via Freidlin-Wentzell large deviation principle of invariant measures*, arXiv:2208.11860, 2022.
- [16] Y. Gao and J.-G. Liu, *Large deviation principle and thermodynamic limit of chemical master equation via nonlinear semigroup*, arXiv:2205.09313, 2022.
- [17] D. T. Gillespie, *A general method for numerically simulating the stochastic time evolution of coupled chemical reactions*, J. Comput. Phys. 22(4) (1976), 403–434.
- [18] D. A. Gomes, *Generalized mather problem and selection principles for viscosity solutions and mather measures*, Adv. Calc. Var. 1(3) (2008), 291–307.
- [19] C. Hartmann and C. Schütte, *Efficient rare event simulation by optimal nonequilibrium forcing*, J. Stat. Mech. Theory Exp. 2012(11) (2012), P11004.
- [20] F. Horn and R. Jackson, *General mass action kinetics*, Arch. Ration. Mech. Anal. 47 (1972), 81–116.
- [21] H. Ishii and A. Siconolfi, *The vanishing discount problem for Hamilton-Jacobi equations in the Euclidean space*, Comm. Partial Differential Equations 45(6) (2020), 525–560.
- [22] R. C. Kraaij, A. Lazarescu, C. Maes, and M. Peletier, *Fluctuation symmetry leads to generic equations with non-quadratic dissipation*, Stochastic Process. Appl. 130(1) (2020), 139–170.

- [23] H. A. Kramers, *Brownian motion in a field of force and the diffusion model of chemical reactions*, *Physica* 7(4) (1940), 284–304.
- [24] R. Kubo, K. Matsuo, and K. Kitahara, *Fluctuation and relaxation of macrovariables*, *J. Stat. Phys.* 9(1) (1973), 51–96.
- [25] T. G. Kurtz, *Limit theorems for sequences of jump Markov processes approximating ordinary differential processes*, *J. Appl. Probab.* 8(2) (1971), 344–356.
- [26] M. Liero, A. Mielke, M. A. Peletier, and D. R. M. Renger, *On microscopic origins of generalized gradient structures*, *Discrete Contin. Dyn. Syst. Ser. S* 10(1) (2017), 1–35.
- [27] C. Lv, X. Li, F. Li, and T. Li, *Constructing the energy landscape for genetic switching system driven by intrinsic noise*, *PLoS One* 9(2) (2014), e88167.
- [28] P. Metzner, C. Schütte, and E. Vanden-Eijnden, *Transition path theory for Markov jump processes*, *Multiscale Model. Simul.* 7(3) (2009), 1192–1219.
- [29] A. Mielke, D. R. M. Renger, and M. A. Peletier, *On the relation between gradient flows and the large-deviation principle, with applications to Markov chains and diffusion*, *Potential Anal.* 41(4) (2014), 1293–1327.
- [30] I. Prigogine, *Introduction to Thermodynamics of Irreversible Processes*, Interscience, 1967.
- [31] H. Qian and H. Ge, *Stochastic Chemical Reaction Systems in Biology*, in: *Lecture Notes on Mathematical Modelling in the Life Sciences*, Springer, 2021.
- [32] H. Qian, M. Qian, and X. Tang, *Thermodynamics of the general diffusion process: Time-reversibility and entropy production*, *J. Stat. Phys.* 107(5) (2002), 1129–1141.
- [33] D. M. Roma, R. A. O’Flanagan, A. E. Ruckenstein, A. M. Sengupta, and R. Mukhopadhyay, *Optimal path to epigenetic switching*, *Phys. Rev. E* 71(1) (2005), 011902.
- [34] F. Schlogl, *Chemical reaction models for non-equilibrium phase transitions*, *Zeitschrift für Physik* 253(2) (1972), 147–161.
- [35] P. J. H. Sharpe and D. W. DeMichele, *Reaction kinetics of poikilotherm development*, *J. Theor. Biol.* 64(4) (1977), 649–670.
- [36] R. Wolfenden, *Analog approaches to the structure of the transition state in enzyme reactions*, *Acc. Chem. Res.* 5(1) (1972), 10–18.